RSC
Medicinal Chemistry

Accepted Manuscript

RSC
Medicinal Chemistry

ROYAL SOCIETY
OF CHEMISTRY

ROYAL SOCIETY
OF CHEMISTRY

rsc.li/medchem

Pegylation Approach Applied to Erlotinib-Carbonic Anhydrase Inhibitors Hybrids Towards Anticancer Agents

Serena Filiberti[a], Gioele Renzi[b,*], Fabrizio Carta[b], Marialuigia Fantacuzzi[c], Ilaria D'Agostino[d], German Benito[b], Andrea Angeli[b], Maria Luisa Massardi[a], Rahime Simsek[e], Clemente Capasso[f], Simone Carradori[c], Roberto Ronca[a] , and Claudiu T. Supuran[b]

[a]Department of Molecular and Translational Medicine, University of Brescia, v.le Europa 11, 25121 Brescia, Italy

[b]NEUROFARBA Department, Pharmaceutical and Nutraceutical section, University of Florence, via Ugo Schiff 6, 50019 Sesto Fiorentino, Italy

[c]Department of Pharmacy, "G. d'Annunzio" University of Chieti and Pescara, via dei Vestini 31, 66100, Chieti, Italy

[d]Department of Pharmacy, University of Pisa, via Bonanno Pisano 6, 56126 Pisa, Italy

[e]Hacettepe University, Faculty of Pharmacy, Department of Pharmaceutical Chemistry, 06100, Sihhiye-Ankara, Turkey

[f]Department of Biology, Agriculture and Food Sciences, National Research Council, Institute of Biosciences & Bioresources, Naples, 80131, Italy

*Corresponding author: Gioele Renzi, gioele.renzi@unifi.it

Abstract

Herein we report a first study on single molecular entities bearing both Epidermal Growth Factor Receptor (EGFR) and Carbonic Anhydrase (CA) Inhibiting moieties as new tools for the management of hypoxic cancers. Specifically, we designed and synthesized a library of Erlotinib (**ERL**)-based compounds bearing both the primary sulfonamide/coumarin moieties with the intent to selectively interfere with EGFR and CA targets respectively. The compounds obtained were investigated *in silico* and in vitro for their ability to interact with the appropriate targets followed by the assessment on selected compounds for the anti-proliferative activity using human (h) TNBC cell line MDA-MB-231. We are confident that the data provided in this study are fundamental for paving the way toward the development of multi-targeting molecular structures useful for the management of chronic diseases such as hypoxic tumors.

Keywords

Erlotinib, carbonic anhydrase, EGFR, coumarin, tumor cells, sulfonamide, PEG linker.

1. INTRODUCTION

Over the years, the definition of cancer has evolved to reflect an increasing understanding of its overall complexity and heterogeneity,[1,2] although data on its morbidity and mortality consistently underscore the ongoing Public Health emergency.[3,4] The current gold standard in cancer treatment, which combines surgery, radiotherapy, and chemotherapy, often faces significant challenges, including limited effectiveness and the associated high failure rates.[5] Recently, the development of immunotherapy and gene-based therapeutics has emerged in response to the urgent need for new effective treatment options, aligning with the rising trend towards personalized medicine.[6] Conversely, the more traditional approach of small molecules in cancer treatment still focuses on modulating enzymatic activities that are crucial for the disease progression and the novelty of the mode of action, in the attempt to avoid cross-resistance phenomena.[7–9] In particular, a valuable strategy consists of anticancer agents endowed with multi-targeted mode of action[10–12] and relies on hybrid compounds[13–17] that combine multiple pharmacophoric features, enabling them to target various pathways and mechanisms simultaneously,[18,19] often spaced by simple flexible linkers as methylene units.[20] In this context, several known anticancer drugs undergo this chemical modification[21–24] and, among them, one of the most employed is Erlotinib (**ERL**, **Figure 1**).[25–32] This small molecule selectively inhibits the epidermal growth factor receptor (EGFR) tyrosine kinase, which is a key player in cell proliferation and disease progression in various cancers, such as non-small cell lung cancer (NSCLC) and pancreatic cancer. [33,34] Mechanistically, **ERL** binds reversibly the tyrosine kinase domain of EGFR, specifically to the ATP-binding site in a competitive manner,[35] thereby, blocking the phosphorylation of EGFR and, consequently, the signaling pathways of PI3K-AKT and RAS-RAF-MEK-ERK,[36–38] mainly involved in tumor growth, survival, and metastasis, along with increased aggressiveness and poor prognosis.[39–41] Interestingly, although the binding to the targeted receptor is governed by relevant networks of interactions also including hydrophobic contacts between the triad of residues (Thr766, leu764, and Lys721) and the acetylene terminal function,[42,43] the latter has often been modified to generate various libraries of compounds, being often employed as starting point for derivatizations[29,30,44–46] with only slight decrease in the inhibitory potency towards EGFR.[44] Specifically, it served for the copper-catalyzed azide-alkyne cycloaddition (CuAAC), a cornerstone of click chemistry, to form the characteristic 1,4-disubstituted 1,2,3-triazole. The introduction of the triazole ring, a known surrogate for amides, esters, and carboxylic acids,[45,47,48] is reported to often increase the affinity for the target, allowing the establishment of additional interactions, such as hydrogen bonds and dipole interactions.[49]

On the other hand, recent findings highlighted the high potential of another family of enzymes in the frame of anticancer treatment development: Carbonic Anhydrases (CAs, EC: 4.2.1.1), being widely reported during the last century due to their ubiquitary nature and their pivotal role in cell
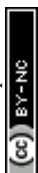
life.[50] These metalloenzymes catalyze the interconversion of carbon dioxide (CO_2) to bicarbonate (HCO_3^-) and proton (H^+), thereby regulating pH and CO_2 homeostasis, electrolyte secretion in various tissues and organs, and other crucial biological processes.[51–53] In particular, the α-CA subfamily is the only one among the identified eight genetically distinct ones (α-, β-, γ- δ-, ζ-, η-, θ-, and ι-CAs) found in humans and is composed of 16 members (I-IV, VA, VB, VI-XV).[50,54] Both the isoforms I and II are physiologically abundant in red blood cells, playing a role in the CO_2 transport, whereas hCA II levels are high also in kidneys, assisting in HCO_3^--resorption and diuresis.[55,56] Conversely, hCAs overexpression is often associated with different diseases, [10,52,57] such as glaucoma for hCA II[58] and hypoxic cancer for isoforms IX[59] and XII,[60] to name but a few. In particular, the latter isozymes were highly exploited and several libraries of CA inhibitors (CAIs), especially bearing the sulfonamide or the coumarin CA inhibiting chemotypes, have been described till now.[61–63]

2. MATERIAL AND METHODS

2.1. Chemistry

2.1.1. General chemistry

Anhydrous solvents and all reagents were purchased from Merck srl, TCI, and Fluorochem. All reactions involving air- or moisture-sensitive compounds were performed under a nitrogen atmosphere using dried glassware and syringes techniques to transfer solutions. Nuclear magnetic resonance (^{1}H- and ^{13}C-NMR) spectra were recorded using a Bruker Advance III 400 MHz spectrometer in DMSO-d_6. Chemical shifts are reported in parts per million (ppm) and the coupling constants (J) are expressed in Hertz (Hz). Splitting patterns are designated as follows: s, singlet; d, doublet; t, triplet; q, quartet; m, multiplet; dd, doublet of doublets; bs, broad singlet; ap s, apparent singlet; ap d, apparent doublet; ap t, apparent triplet; ap q, apparent quartet. The assignment of exchangeable protons (OH and NH) was confirmed by the addition of D_2O. Analytical thin-layer chromatography (TLC) was carried out on Merck silica gel F-254 plates. Flash chromatography purifications were performed on Merck silica gel 60 (230-400 mesh ASTM) as the stationary phase and methanol/dichloromethane (MeOH/DCM) or ethyl acetate/hexane (EtOAc/Hex) was used as eluents. The solvents used in Mass Spectrometry (MS) measures were acetone, acetonitrile (Chromasolv grade), and 56 mQ water 18 MΩ, obtained from Millipore's Simplicity system (Milan-Italy). The mass spectra were obtained using a Varian 1200L triple quadrupole system (Palo Alto, USA) equipped with Electrospray Source (ESI) operating in both positive and negative modes. Stock solutions of analytes were prepared in acetone at 1.0 mg mL^{-1} and stored at 4 ºC. Working solutions of each analyte were freshly prepared by diluting stock solutions in a mixture of mQ H_2O/ACN 1/1(v/v) up to a concentration of 1.0 µg/mL. The MS spectra of each analyte were acquired by introducing, via a syringe pump at 10 L/min, the working solution. RawQdata were collected and processed by Varian Workstation Vers. 6.8.

2.1.2. General procedure for the synthesis of compounds 19a and 19b

The appropriate sulfonamide **16a**[103] or **16b**[104] (1 equiv) and the commercial 2-(2-(2-(2-azidoethoxy)ethoxy)ethoxy)ethan-1-amine **15** (1.2 equiv) were dissolved in ACN (10 mL) and the reaction mixture was stirred at reflux temperature overnight. Then, slush was added to quench the reaction and extracted with EtOAc thrice. The combined organic layers were dried over anhydrous Na_2SO_4, filtered, and evaporated at reduced pressure to yield compounds **19a** or **19b**.

3-(3-(2-(2-(2-(2-azidoethoxy)ethoxy)ethoxy)ethyl)ureido)benzenesulfonamide (19a)

Yellow oil. Yield: 65%. **¹H NMR (400 MHz, DMSO-d_6) δ (ppm):** 8.00 (1H, s, N*H*, exchange with D_2O), 7.54 (1H, d, *J* = 7.50 Hz), 7.42 (t, 1H, *J* = 7.55 Hz, N*H*, exchange with D_2O), 7.19 (2H, t, *J* = 7.76 Hz), 6.79 (2H, bs, SO_2NH_2, exchange with D_2O), 6.28 (1H, t, *J* = 5.37 Hz), 3.62 (2H, t, *J* = 3.77 Hz), 3.58 (8H, m), 3.50 (2H, t, *J* = 5.37 Hz), 3.41 (2H, m), 3.30 (2H, m). **¹³C NMR (100 MHz, DMSO-d_6) δ (ppm):** 154.3, 139.9, 136.2, 127.0, 124.8, 122.9, 119.8, 70.4, 70.3, 70.2, 70.1, 70.0, 69.7, 50.0, 41.5; MS (ESI positive) *m/z*: 417.15 [M+H]⁺. Elemental analysis: calculated C, 43.26; H, 5.81; N, 20.18; found C, 43.25; H, 5.82; N, 20.16.

4-(3-(2-(2-(2-(2-azidoethoxy)ethoxy)ethoxy)ethyl)ureido)benzenesulfonamide (19b)

Yellow oil. Yield: 60%. **¹H NMR (400 MHz, DMSO-d_6) δ (ppm):** 8.02 (1H, s, N*H*, exchange with D_2O), 7.72 (2H, d, *J* = 7.89 Hz), 7.57 (2H, d, *J* = 7.89 Hz), 6.80 (2H, bs, SO_2NH_2, exchange with D_2O), 6.36 (1H, t, *J* = 5.56 Hz, N*H*, exchange with D_2O), 3.63 (3H, t, *J* = 4.79 Hz), 3.59 (8H, s), 3.42 (3H, m), 3.30 (2H, q, *J* = 6.12 Hz). **¹³C NMR (100 MHz, DMSO-d_6) δ (ppm):** 154.3, 142.6, 136.5, 129.5, 129.4, 118.1, 118.0, 70.4, 70.3, 70.2, 70.1, 70.0, 69.7, 50.0, 41.5; MS (ESI positive) *m/z*: 417.15 [M+H]⁺. Elemental analysis: calculated C, 43.26; H, 5.81; N, 20.18; found C, 43.25; H, 5.82; N, 20.19.

2.1.3. General procedure for the synthesis of compounds 20a-d and 21

The appropriate sulfonamide **17a-d**[105–107] or **18**[108] (1 equiv) and the commercial 2-(2-(2-(2-azidoethoxy)ethoxy)ethoxy)ethan-1-amine **15** (1.2 equiv) were dissolved in ACN (10 mL) and the reaction mixture was stirred at room temperature overnight. Then, slush added to quench the reaction and extracted with EtOAc thrice. The combined organic layers were dried over anhydrous Na_2SO_4, filtered, and evaporated at reduced pressure to yield compounds **20a-d** and **21**.

3-(3-(2-(2-(2-(2-azidoethoxy)ethoxy)ethoxy)ethyl)thioureido)benzenesulfonamide (20a)

Yellow oil. Yield: 95%. **¹H NMR (400 MHz, DMSO-d_6) δ (ppm):** 9.94 (1H, s, N*H*, exchange with D_2O), 7.99 (2H, d, *J* = 18.6 Hz), 7.76 (1H, d, *J* = 7.11 Hz), 7.55 (2H, bs, SO_2NH_2, exchange with D_2O), 7.40 (1H, s, N*H*, exchange with D_2O), 4.06 (2H, d, *J* = 7.22 Hz), 3.60 (14H, m). **¹³C NMR (100 MHz, DMSO-d_6) δ (ppm):** 179.5, 140.0, 137.4, 129.7, 127.1, 124.7 123.3, 70.6, 70.5, 70.4, 70.2, 70.1, 70.0, 50.0, 45.3; MS (ESI positive) *m/z*: 433.13 [M+H]⁺. Elemental analysis: calculated C, 41.66; H, 5.59; N, 19.43; found C, 41.64; H, 5.58; N, 19.45.

4-(3-(2-(2-(2-(2-azidoethoxy)ethoxy)ethoxy)ethyl)thioureido)benzenesulfonamide (20b)

Yellow oil. Yield: 95%. **¹H NMR (400 MHz, DMSO-d_6) δ (ppm):** 9.97 (1H, s, N*H*, exchange with D_2O), 8.01 (1H, s, N*H*, exchange with D_2O), 7.74 (4H, q, *J* = 8.07 Hz), 7.31 (2H, bs, SO_2NH_2,

exchange with D_2O), 3.61 (16H, m). **^{13}C NMR (100 MHz, DMSO-d_6) δ (ppm):** 179.5, 141.7, 136.9, 129.6, 129.5, 122.9, 122.8, 70.5, 70.4, 70.3, 70.2, 70.1, 70.0, 50.0, 45.3; MS (ESI positive) m/z: 433.13 [M+H]$^+$. Elemental analysis: calculated C, 41.66; H, 5.59; N, 19.43; found C, 41.65; H, 5.58; N, 19.44.

4-(15-azido-3-thioxo-7,10,13-trioxa-2,4-diazapentadecyl)benzenesulfonamide (20c)

Yellow oil. Yield: 97%. **^1H NMR (400 MHz, DMSO-d_6) δ (ppm):** 8.10 (1H, s, N*H*, exchange with D_2O), 7.80 (2H, d, J = 7.59 Hz), 7.67 (1H, s, N*H*, exchange with D_2O), 7.47 (2H, d, J = 7.59 Hz), 7.35 (2H, bs, SO_2NH_2, exchange with D_2O), 4.77 (2H, s), 4.07 (2H, d, J = 6.51 Hz), 3.58 (14H, m). **^{13}C NMR (100 MHz, DMSO-d_6) δ (ppm):** 182.3, 141.7, 141.1, 128.3, 128.2, 127.3, 127.2, 70.6, 70.5, 70.4, 70.2, 70.1, 70.0, 50.8, 50.0, 45.3; MS (ESI positive) m/z: 447.14 [M+H]$^+$. Elemental analysis: calculated C, 43.04; H, 5.87; N, 18.82; found C, 43.05; H, 5.86; N, 18.83.

4-(16-azido-4-thioxo-8,11,14-trioxa-3,5-diazahexadecyl)benzenesulfonamide (20d)

Yellow oil. Yield: 97%. **^1H NMR (400 MHz, DMSO-d_6) δ (ppm):** 7.79 (2H, d, J = 7.59 Hz), 7.60 (1H, s, N*H*, exchange with D_2O), 7.54 (1H, s, N*H*, exchange with D_2O), 7.45 (2H, d, J = 7.59 Hz), 7.34 (2H, bs, SO_2NH_2, exchange with D_2O), 3.64 (5H, m), 3.57 (14H, m), 2.92 (2H, m). **^{13}C NMR (100 MHz, DMSO-d_6) δ (ppm):** 181.8, 142.6, 140.9, 128.4, 128.3, 128.1, 128.0, 70.5, 70.4, 70.3, 70.2, 70.1, 70.0, 50, 47.8, 45.3, 35.3; MS (ESI positive) m/z: 461.16 [M+H]$^+$. Elemental analysis: calculated C, 44.33; H, 6.13; N, 18.25; found C, 44.34; H, 6.12; N, 18.26.

4-(3-(2-(2-(2-(2-azidoethoxy)ethoxy)ethoxy)ethyl)thioureido)-3-bromo-2-methylbenzenesulfonamide (21)

Yellow oil. Yield: 75%. ^1H NMR (400 MHz, DMSO-d_6) δ (ppm): 9.40 (1H, s, NH, exchange with D_2O), 8.44 (1H, s), 8.05 (1H, s), 7.51 (2H, bs, SO_2NH_2, exchange with D_2O), 7.28 (1H, s, NH, exchange with D_2O), 4.14 (2H, q, J = 5.19 Hz), 3.61 (8H, m), 3.21 (5H, m). ^{13}C NMR (100 MHz, DMSO-d_6) δ (ppm): 179.5, 140.3, 138.3, 137.1, 126.5, 126.0, 120.9, 70.5, 70.4, 70.1, 70.4, 70.0, 50.0, 45.3, 13.6; MS (ESI positive) m/z: 525.05 [M+H]$^+$. Elemental analysis: calculated C, 36.57; H, 4.80; N, 15.99; found C, 36.58; H, 4.81; N, 15.97.

General procedure for the synthesis of compounds 7a-d, 8a-d, and 9

Erlotinib Hydrochloride (**ERL**) (1 equiv), copper nanosized (0.5 equiv), tetramethylammonium chloride (4.5 equiv) and the appropriate azide derivative **19-21** (1.2 equiv) were dissolved in DMF (2.5 mL) and stirred overnight at 60 °C. Then, the reaction mixture was filtered through a cake of Celite 521$^©$ and the filtrate was treated with slush. The crude was and extracted with DCM thrice. The combined organic layers were dried over anhydrous Na_2SO_4, filtered, and evaporated at reduced pressure. The crude material was purified by flash column chromatography (MeOH/DCM: 5:95), to yield compounds **7a-b**, **8a-d**, and **9**.

3-(3-(2-(2-(2-(2-(4-(3-((6,7-bis(2-methoxyethoxy)quinazolin-4-yl)amino)phenyl)-1*H*-1,2,3-triazol-1-yl)ethoxy)ethoxy)ethoxy)ethyl)ureido)benzenesulfonamide (7a)

Yellow oil. Yield: 5%. **¹H NMR (400 MHz, DMSO-*d*₆) *δ* (ppm):** 9.58 (1H, s, N*H*, exchange with D₂O), 8.90 (1H, s), 8.54 (1H, s), 8.48 (1H, s), 8.28 (1H, s, N*H*, exchange with D₂O), 7.95 (2H, d, *J* = 10.52 Hz), 7.88 (1H, d, *J* = 7.94 Hz), 7.55 (1H, d, *J* = 7.57 Hz), 7.48 (2H, t, *J* = 8.31 Hz), 7.38 (1H, t, *J* = 7.79 Hz), 7.33 (1H, d, *J* = 7.74 Hz), 7.29 (2H, bs, SO₂N*H₂*, exchange with D₂O), 7.23 (1H, s), 6.24 (1H, t, *J* = 5.23 Hz), 4.58 (2H, t, *J* = 4.63 Hz), 4.31 (4H, m), 3.88 (2H, t, *J* = 4.72 Hz), 3.79 (2H, m), 3.75 (2H, m), 3.45 (16H, m), 3.21 (2H, m). **¹³C NMR (100 MHz, DMSO-*d*₆) *δ* (ppm):** 156.4, 154.9, 153.6, 152.9, 148.1, 146.9, 146.2, 144.5, 140.9, 140.0, 131.0, 129.2, 129.0, 121.8, 121.7, 120.3, 118.7, 118.0, 114.4, 108.9, 108.1, 103.2, 101.8, 70.1, 70.0, 69.7, 69.6 ,68.6, 68.3, 68.0, 58.4, 58.3, 49.6, 28.9; MS (ESI positive) *m/z*: 810.32 [M+H]⁺. Elemental analysis: calculated C, 54.87; H, 5.85; N, 15.57; found C, 54.88; H, 5.84; N, 15.55.

4-(3-(2-(2-(2-(2-(4-(3-((6,7-bis(2-methoxyethoxy)quinazolin-4-yl)amino)phenyl)-1*H*-1,2,3-triazol-1-yl)ethoxy)ethoxy)ethoxy)ethyl)ureido)benzenesulfonamide (7b)

Yellow oil. Yield: 19%. **¹H NMR (400 MHz, DMSO-*d*₆) *δ* (ppm):** 9.59 (1H, s, N*H*, exchange with D₂O), 8.96 (1H, s), 8.55 (1H, s), 8.48 (1H, s), 8.27 (1H, s), 7.93 (1H, s, N*H*, exchange with D₂O), 7.88 (1H, d, *J* = 7.65 Hz), 7.65 (2H, d, *J* = 8.29 Hz), 7.55 (1H, d, *J* = 7.8 Hz), 7.51 (2H, d, *J* = 8.76 Hz), 7.46 (1H, t, *J* = 7.87 Hz), 7.23 (1H, s), 7.17 (2H, bs, SO₂N*H₂*, exchange with D₂O), 6.31 (1H, t, *J* = 5.4 Hz), 4.58 (2H, t, *J* = 4.94 Hz), 4.30 (4H, m), 3.87 (2H, t, *J* = 5.0 Hz), 3.79 (2H, m), 3.75 (2H, m), 3.52 (8H, m), 3.36 (6H, m), 3.21 (2H, m), 3.16 (2H, d, *J* = 5.17 Hz). **¹³C NMR (100 MHz, DMSO-*d*₆) *δ* (ppm):** 156.4, 154.7, 153.6, 152.9, 148.1, 146.9, 146.2, 143.6, 140.0, 136.0, 131.0, 129.0, 126.8, 121.8, 121.7, 120.3, 118.7, 116.7, 108.9, 108.1, 103.2, 70.1, 70.0, 69.7, 69.6, 68.6, 68.3, 68.0, 58.4, 58.3, 49.6, 48.6; MS (ESI positive) *m/z*: 810.32 [M+H]⁺. Elemental analysis: calculated C, 54.87; H, 5.85; N, 15.57; found C, 54.89; H, 5.86; N, 15.56.

3-(3-(2-(2-(2-(2-(4-(3-((6,7-bis(2-methoxyethoxy)quinazolin-4-yl)amino)phenyl)-1*H*-1,2,3-triazol-1-yl)ethoxy)ethoxy)ethoxy)ethyl)thioureido)benzenesulfonamide (8a)

Yellow oil. Yield: 27%. **¹H NMR (400 MHz, DMSO-*d*₆) *δ* (ppm):** 9.86 (1H, m, N*H*, exchange with D₂O), 9.57 (1H, s), 8.54 (1H, s), 8.48 (1H, m), 8.28 (1H, s, N*H*, exchange with D₂O), 7.96 (1H, m), 7.93 (1H, s), 7.88 (1H, d, *J* = 7.18 Hz), 7.70 (1H, d, *J* = 7.33 Hz), 7.53 (2H, t, *J* = 7.98 Hz), 7.46 (2H, m), 7.36 (2H, bs, SO₂N*H₂*, exchange with D₂O), 7.23 (1H, m), 4.59 (2H, t, *J* = 4.93 Hz), 4.30 (4H, m), 3.88 (2H, t, *J* = 5.19 Hz), 3.79 (3H, t, *J* = 4.94 Hz), 3.75 (3H, m), 3.50 (12H, m), 3.37 (4H, m). **¹³C NMR (100 MHz, DMSO-*d*₆) *δ* (ppm):** 181.4, 180.6, 165.4, 156.4, 153.6, 153.0, 148.1, 147.0, 146.8, 146.2, 144.3, 140.0, 131.1, 134.7, 129.0, 125.7, 121.9, 121.8, 120.3, 118.8, 108.1, 103.2, 70.1, 70.0, 69.7, 69.6, 68.7, 68.4, 68.0, 58.4, 58.3, 49.6, 48.6, 43.6; MS (ESI positive) *m/z*: 826.30 [M+H]⁺. Elemental analysis: calculated C, 53.81; H, 5.74; N, 15.26; found C, 53.82; H, 5.73; N, 15.24.

4-(3-(2-(2-(2-(2-(4-(3-((6,7-bis(2-methoxyethoxy)quinazolin-4-yl)amino)phenyl)-1*H*-1,2,3-triazol-1-yl)ethoxy)ethoxy)ethoxy)ethyl)thioureido)benzenesulfonamide (8b)

Yellow oil. Yield: 35%. **¹H NMR (400 MHz, DMSO-*d₆*) *δ* (ppm):** 9.64 (1H, s, N*H*, exchange with D₂O), 8.55 (1H, s), 8.50 (1H, s), 8.28 (1H, s), 8.09 (1H, s N*H*, exchange with D₂O), 7.96 (1H, s), 7.88 (1H, d, *J* = 7.34 Hz), 7.76 (2H, d, *J* = 9.15 Hz), 7.66 (1H, m), 7.55 (1H, m), 7.47 (1H, d, *J* = 7.92 Hz), 7.41 (1H, d, *J* = 7.92 Hz), 7.32 (2H, bs, SO₂N*H₂*, exchange with D₂O), 7.24 (1H, s), 4.72 (2H, m), 4.59 (2H, m) 4.30 (4H, m), 4.13 (2H, m), 3.88 (2H, t, *J* = 5.09 Hz), 3.79 (2H, m), 3.75 (2H, m), 3.55 (3H, m), 3.52 (10H, m), 3.16 (3H, d, *J* = 4.85 Hz). **¹³C NMR (100 MHz, DMSO-*d₆*) *δ* (ppm):** 185.4, 156.3, 154.8, 146.2, 140.0, 136.0, 131.0, 129.4, 129.0, 127.0, 126.7, 121.8, 120.7, 118.7, 116.7, 103.3, 90.2, 70.1, 69.9, 69.7, 69.6, 69.1, 68.6, 68.0, 65.3, 61.9, 60.2, 58.4, 49.7, 49.6, 29.0; MS (ESI positive) *m*/*z*: 826.30 [M+H]⁺. Elemental analysis: calculated C, 53.81; H, 5.74; N, 15.26; found C, 53.79; H, 5.75; N, 15.28.

4-(15-(4-(3-((6,7-bis(2-methoxyethoxy)quinazolin-4-yl)amino)phenyl)-1*H*-1,2,3-triazol-1-yl)-3-thioxo-7,10,13-trioxa-2,4-diazapentadecyl)benzenesulfonamide (8c)

Yellow oil. Yield: 42%. **¹H NMR (400 MHz, DMSO-*d₆*) *δ* (ppm):** 9.64 (1H, m, N*H*, exchange with D₂O), 8.59 (1H, s), 8.32 (1H, s), 8.00 (1H, s, N*H*, exchange with D₂O), 7.90 (1H, d, *J* = 7.38 Hz), 7.80 (2H, d, *J* = 7.72 Hz), 7.59 (1H, d, *J* = 7.72 Hz), 7.51 (1H, d, *J* = 8.13 Hz), 7.46 (2H, d, *J* = 7.72 Hz), 7.35 (2H, bs, SO₂N*H₂*, exchange with D₂O), 7.33 (1H, m), 4.62 (2H, m), 4.34 (5H, m), 3.92 (2H, m), 3.81 (5H, m), 3.54 (14H, m), 3.41 (8H, m). **¹³C NMR (100 MHz, DMSO-*d₆*) *δ* (ppm):** 163.2, 156.4, 155.8, 153.6, 152.8, 148.1, 146.8, 146.2, 142.5, 140.0, 137.6, 131.1, 129.0, 127.8, 127.4, 125.6, 121.8, 120.3, 118.8, 108.1, 103.3, 70.1, 70.0, 69.7, 69.6, 68.8, 68.6, 68.4, 68.0, 58.4, 58.4, 49.6, 48.6; MS (ESI positive) *m*/*z*: 840.31 [M+H]⁺. Elemental analysis: calculated C, 53.98; H, 5.78; N, 15.18; found C, 53.99; H, 5.79; N, 15.16.

4-(16-(4-(3-((6,7-bis(2-methoxyethoxy)quinazolin-4-yl)amino)phenyl)-1*H*-1,2,3-triazol-1-yl)-4-thioxo-8,11,14-trioxa-3,5-diazahexadecyl)benzenesulfonamide (8d)

Yellow oil. Yield: 72%. **¹H NMR (400 MHz, DMSO-*d₆*) *δ* (ppm):** 9.69 (1H, m, N*H*, exchange with D₂O), 8.55 (2H, m), 8.28 (1H, s), 7.94 (1H, s, N*H*, exchange with D₂O), 7.84 (1H, m), 7.75 (3H, m), 7.57 (1H, d, *J* = 7.51 Hz), 7.48 (1H, m), 7.42 (3H, m), 7.32 (2H, bs, SO₂N*H₂*, exchange with D₂O), 7.32 (1H, s), 4.58 (2H, m), 4.30 (4H, m), 3.87 (2H, m), 3.79 (2H, m), 3.75 (2H, m), 3.49 (16H, m), 3.35 (4H, m), 2.88 (2H, m). **¹³C NMR (100 MHz, DMSO-*d₆*) *δ* (ppm):** 190.0, 158.9, 158.3, 153.7, 148.3, 148.2, 146.5, 146.2, 143.4, 142.2, 131.1, 129.7, 129.3, 129.2, 126.3, 126.0, 125.7, 122.5, 121.9, 103.2, 80.2, 70.1, 70.0, 69.7, 69.6, 69.3, 68.9, 68.7, 68.4, 68.1, 58.4, 58.3, 50.0, 49.6; MS (ESI positive) *m*/*z*: 854.33 [M+H]⁺. Elemental analysis: calculated C, 54.85; H, 6.02; N, 14.76; found C, 54.84; H, 6.01; N, 14.78.

4-(3-(2-(2-(2-(2-(4-(3-((6,7-bis(2-methoxyethoxy)quinazolin-4-yl)amino)phenyl)-1*H*-1,2,3-triazol-1-yl)ethoxy)ethoxy)ethoxy)ethyl)thioureido)-3-bromo-2-methylbenzenesulfonamide (9)

Yellow oil. Yield: 46%. **¹H NMR (400 MHz, DMSO-*d₆*) *δ* (ppm):** 9.57 (1H, s, N*H*, exchange with D₂O), 8.53 (1H, s), 8.46 (2H, m), 8.28 (1H, s), 8.11 (1H, m), 7.93 (1H, s, N*H*, exchange with D₂O),
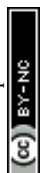
7.88 (1H, d, J = 8.26 Hz), 7.65 (1H, d, J = 8.68 Hz), 7.54 (1H, d, J = 7.44 Hz), 7.46 (2H, m), 7.23 (1H, s), 7.20 (2H, bs, SO$_2$NH_2, exchange with D$_2$O), 4.58 (2H, m), 4.31 (4H, m), 3.87 (2H, t, J = 5.37 Hz), 3.79 (2H, t, J = 4.22 Hz), 3.75 (2H, t, J = 4.21 Hz), 3.54 (8H, m), 3.45-3.40 (9H, m).^{13}C NMR (100 MHz, DMSO-d_6) δ(ppm): 182.2, 180.4, 175.7, 173.9, 172.0, 168.6, 152.9, 147.3, 144.8, 141.6, 140.1, 138.7, 134.5, 130.3, 121.8, 120.2, 119.0, 117.3, 116.2, 112.4, 107.8, 105.5, 103.3, 75.3, 70.0, 69.6, 68.5, 68.3, 68.0, 67.3, 63.4, 58.3, 55.3, 46.8, 31.9; MS (ESI positive) m/z: 918.22 [M+H]$^+$. Elemental analysis: calculated C, 52.17; H, 5.63; N, 14.22; found C, 52.18; H, 5.64; N, 14.21.

General procedure for the synthesis of compounds 25a-b and 26

The commercially available sulfonamide **23a**,**b** or coumarin **24**[109] (1 equiv), commercially available 2,5-dioxopyrrolidin-1-yl 1-azido-3,6,9,12,15-pentaoxaoctadecan-18-oate **22** (1.1 equiv, azido-PEG5-NHS ester) and DIPEA (1.5 equiv) were dissolved in DMF (5 mL) and the reaction mixture was stirred at room temperature overnight. Then, the reaction mixture was treated with slush and aq. NH$_4$Cl, extracted with EtOAc thrice. The combined organic layers were dried over anhydrous Na$_2$SO$_4$, filtered, and evaporated at reduced pressure. The crude material was purified by flash column chromatography (MeOH/DCM: 5:95), to yield compounds **25a-b** and **26**.

1-azido-N-(4-sulfamoylbenzyl)-3,6,9,12,15-pentaoxaoctadecan-18-amide (25a)

Yellow oil. Yield: 61%. **^{1}H NMR (400 MHz, DMSO-d_6) δ (ppm):** 8.45 (1H, t, J = 5.32 Hz, NH, exchange with D$_2$O), 7.75 (2H, d, J = 8.20 Hz), 7.41 (2H, d, J = 7.91 Hz), 7.30 (2H, bs, SO$_2$NH_2, exchange with D$_2$O), 4.33 (2H, d, J = 5.73 Hz), 3.63 (2H, t, J = 7.09 Hz), 3.60 (2H, t, J = 4.84 Hz), 3.50 (16H, m), 3.38 (2H, t, J = 4.91 Hz), 2.39 (2H, t, J = 6.09 Hz). **^{13}C NMR (100 MHz, DMSO-d_6) δ (ppm):** 174.3, 142.3, 138.2, 130.3, 129.2, 70.6, 70.4, 69.5, 68.4, 49.1, 45.8, 25.9; MS (ESI positive) m/z: 504.2 [M+H]$^+$. Elemental analysis: calculated C, 47.70; H, 6.61; N, 13.91; found C, 47.71; H, 6.62; N, 13.90.

1-azido-N-(4-sulfamoylphenethyl)-3,6,9,12,15-pentaoxaoctadecan-18-amide (25b)

Yellow oil. Yield: 49%. **^{1}H NMR (400 MHz, DMSO-d_6) δ (ppm):** 7.93 (1H, t, J = 5.70 Hz, NH, exchange with D$_2$O), 7.73 (2H, d, J = 8.15 Hz), 7.38 (2H, d, J = 8.15 Hz), 7.28 (2H, bs, SO$_2$NH_2, exchange with D$_2$O), 3.58 (4H, m), 3.53 (4H, m), 3.49 (8H, m), 3.47 (4H, m), 3.38 (2H, t, J = 5.14 Hz), 3.27 (2H, t, J = 6.14 Hz), 2.77 (2H, t, J = 7.14 Hz), 2.28 (2H, t, J = 6.42 Hz). **^{13}C NMR (100 MHz, DMSO-d_6) δ (ppm):** 179.3, 142.5, 133.8, 130.9, 128.5, 71.4, 70.6, 70.4, 69.1, 67.3, 45.4, 42.7, 37.4, 30.4; MS (ESI positive) m/z: 517.22 [M+H]$^+$. Elemental analysis: calculated C, 48.73; H, 6.82; N, 13.53; found C, 48.72; H, 6.83; N, 13.54.

1-azido-N-(2-((2-oxo-2H-chromen-6-yl)oxy)ethyl)-3,6,9,12,15-pentaoxaoctadecan-18-amide (26)

Yellow oil. Yield: 70%. **^{1}H NMR (400 MHz, DMSO-d_6) δ (ppm):** 8.12 (1H, t, J = 5.82 Hz, NH, exchange with D$_2$O), 8.00 (1H, d, J = 9.41 Hz), 7.34 (1H, d, J = 9.09 Hz), 7.30 (1H, d, J = 2.76 Hz), 7.20 (1H, dd, J = 8.08, 9.02 Hz), 6.49 (1H, d, J = 9.61 Hz), 4.02 (2H, t, J = 5.64 Hz), 3.58 (4H, m),

3.52 (4H, m), 3.49 (4H, m), 3.45 (10H, m), 3.38 (2H, t, J = 4.73 Hz), 2.34 (2H, t, J = 6.20 Hz). ^{13}C NMR (100 MHz, DMSO-d_6) δ (ppm): 171.9, 165.2, 158.1, 154.7, 142.0, 119.3, 115.2, 113.4, 111.5, 71.3, 70.8, 70.6, 70.3, 69.8, 65.5, 61.4, 48.1, 39.3, 29.2; MS (ESI positive) m/z: 523.2 [M+H]$^+$. Elemental analysis: calculated C, 55.16; H, 6.56; N, 10.72; found C, 55.17; H, 6.55; N, 10.71.

2.1.4. General procedure for the synthesis of compounds 29a-c

The appropriate sulfonamide **16a-c**[105] (1 equiv) and 17-azido-3,6,9,12,15-pentaoxaheptadecan-1-amine **27** (1.1 equiv) were dissolved in ACN (10 mL) and the reaction mixture was stirred at reflux temperature overnight. Then, the reaction mixture was treated with slush and extracted with EtOAc thrice. The combined organic layers were dried over anhydrous Na$_2$SO$_4$, filtered, and evaporated at reduced pressure. The crude material was purified by flash column chromatography (MeOH/DCM: 5:95), to yield compounds **29a-c**.

3-(3-(17-azido-3,6,9,12,15-pentaoxaheptadecyl)ureido)benzenesulfonamide (29a)

Yellow oil. Yield: 67%. ^{1}H NMR (400 MHz, DMSO-d_6) δ (ppm): 8.88 (1H, s, NH, exchange with D$_2$O), 7.96 (1H, s, NH, exchange with D$_2$O), 7.50 (1H, d, J = 7.51 Hz), 7.39 (1H, t, J = 7.93 Hz), 7.33 (1H, d, J = 7.51 Hz), 7.28 (2H, bs, SO$_2$NH_2, exchange with D$_2$O), 6.24 (1H, t, J = 5.18 Hz), 3.59 (2H, t, J = 4.47 Hz), 3.52 (16H, m), 3.46 (2H, t, J = 5.35 Hz), 3.38 (2H, t, J = 4.07 Hz), 3.26 (2H, m). ^{13}C NMR (100 MHz, DMSO-d_6) δ (ppm): 155.6, 145.1, 141.4, 130.0, 121.2, 118.9, 115.1, 70.4, 70.3, 70.2, 69.9, 50.7, 31.3; MS (ESI positive) m/z: 505.1 [M+H]$^+$. Elemental analysis: calculated C, 45.23; H, 6.39; N, 16.66; found C, 45.22; H, 6.38; N, 16.67.

4-(3-(17-azido-3,6,9,12,15-pentaoxaheptadecyl)ureido)benzenesulfonamide (29b)

Yellow oil. Yield: 32%. ^{1}H NMR (400 MHz, DMSO-d_6) δ (ppm): 8.95 (1H, s, NH, exchange with D$_2$O), 7.66 (2H, d, J = 8.27 Hz), 7.52 (2H, d, J = 9.05 Hz), 7.14 (2H, bs, SO$_2$NH_2, exchange with D$_2$O), 6.32 (1H, t, J = 5.51 Hz, NH, exchange with D$_2$O), 3.58 (2H, t, J = 5.11 Hz), 3.52 (16H, m), 3.46 (2H, t, J = 5.38 Hz), 3.38 (2H, t, J = 4.69 Hz), 3.25 (2H, dt, J = 10.71, 11.34 Hz). ^{13}C NMR (100 MHz, DMSO-d_6) δ (ppm): 159.8, 143.7, 137.4, 130.6, 128.1, 70.6, 70.4, 70.5, 69.4, 50.2, 46.3; MS (ESI positive) m/z: 527.2 [M+H]$^+$. Elemental analysis: calculated C, 45.23; H, 6.39; N, 16.66; found C, 45.21; H, 6.40; N, 16.68.

4-(21-azido-3-oxo-7,10,13,16,19-pentaoxa-2,4-diazahenicosyl)benzenesulfonamide (29c)

Yellow oil. Yield: 52%. ^{1}H NMR (400 MHz, DMSO-d_6) δ (ppm): 7.75 (2H, d, J = 8.27 Hz), 7.39 (2H, d, J = 8.27 Hz), 7.26 (2H, bs, SO$_2$NH_2, exchange with D$_2$O), 6.51 (1H, t, J = 6.39 Hz, NH, exchange with D$_2$O), 6.02 (1H, t, J = 4.88 Hz, NH, exchange with D$_2$O), 4.25 (2H, d, J = 5.26 Hz), 3.59 (2H, t, J = 5.13 Hz), 3.52 (16H, m), 3.38 (4H, m), 3.17 (2H, t, J = 5.47 Hz). ^{13}C NMR (100 MHz, DMSO-d_6) δ (ppm): 163.7, 142.3, 137.4, 129.4, 129.1, 128.5, 71.7, 70.8, 70.6, 70.4, 67.3, 65.9, 50.2, 45.6, 44.9; MS (ESI positive) m/z: 519.2 [M+H]$^+$. Elemental analysis: calculated C, 45.60; H, 6.47; N, 16.50; found C, 45.61; H, 6.48; N, 16.49.

2.1.5. General procedure for the synthesis of compounds 32b-d

The appropriate sulfonamide **17b-d** (1 equiv) and the commercial 17-azido-3,6,9,12,15-pentaoxaheptadecan-1-amine **27** (1.1 equiv) were dissolved in ACN (5 mL). K_2CO_3 (1.5 equiv) was then added, and the reaction mixture was stirred at room temperature overnight. Then, the reaction mixture was treated with slush and aq. NH_4Cl, extracted with EtOAc thrice. The combined organic layers were dried over anhydrous Na_2SO_4, filtered, and evaporated at reduced pressure. The crude material was purified by flash column chromatography (MeOH/DCM: 5:95), to yield compounds **18b-d**.

4-(3-(17-azido-3,6,9,12,15-pentaoxaheptadecyl)thioureido)benzensulfonamide (32b)

Yellow oil. Yield: 67%. **^{1}H NMR (400 MHz, DMSO-d_6) δ (ppm):** 9.92 (1H, s, N*H*, exchange with D_2O), 8.02 (1H, s, N*H*, exchange with D_2O), 7.72 (2H, d, *J* = 8.69 Hz), 7.67 (2H, d, *J* = 8.99 Hz), 7.26 (2H, bs, SO_2NH_2, exchange with D_2O), 3.64 (2H, m), 3.59 (5H, m), 3.54 (15H, m), 3.38 (2H, t, *J* = 4.71 Hz). **^{13}C NMR (100 MHz, DMSO-d_6) δ (ppm):** 179.2, 140.1, 138.7, 129.1, 119.6, 119.5, 71.1, 70.8, 70.6, 69.8, 65.8, 50.2, 44.7; MS (ESI positive) *m/z*: 521.2 $[M+H]^+$. Elemental analysis: calculated C, 43.83; H, 6.20; N, 16.14; found C, 43.82; H, 6.21; N, 16.12.

4-(21-azido-3-thioxo-7,10,13,16,19-pentaoxa-2,4-diazahenicosyl)benzenesulfonamide (32c)

Yellow oil. Yield: 63%. **^{1}H NMR (400 MHz, DMSO-d_6) δ (ppm):** 8.03 (1H, s, N*H*, exchange with D_2O), 7.75 (2H, d, *J* = 8.39 Hz), 7.63 (1H, s, N*H*, exchange with D_2O), 7.42 (2H, d, *J* = 8.44 Hz), 7.31 (2H, bs, SO_2NH_2, exchange with D_2O), 4.73 (2H, m), 3.54 (22H, m), 3.38 (2H, t, *J* = 5.26 Hz). **^{13}C NMR (100 MHz, DMSO-d_6) δ (ppm):** 168.9, 146.7, 136.2, 127.4, 124.7, 70.9, 70.7, 70.6, 69.3, 63.5, 47.5, 46.3, 44.4; MS (ESI positive) *m/z*: 535.1 $[M+H]^+$. Elemental analysis: calculated C, 44.39; H, 6.30; N, 15.93; found C, 44.38; H, 6.31; N, 15.94.

4-(22-azido-4-thioxo-8,11,14,17,20-pentaoxa-3,5-diazadocosyl)benzenesulfonamide (32d)

Yellow oil. Yield: 60%. **^{1}H NMR (400 MHz, DMSO-d_6) δ (ppm):** 7.74 (2H, d, *J* = 8.20 Hz), 7.53 (1H, s, N*H*, exchange with D_2O), 7.47 (1H, s, N*H*, exchange with D_2O), 7.41 (2H, d, *J* = 8.11 Hz), 7.29 (2H, bs, SO_2NH_2, exchange with D_2O), 3.59 (3H, t, *J* = 4.22 Hz), 3.51 (21H, m), 3.38 (2H, t, *J* = 4.87 Hz), 2.87 (2H, t, *J* = 7.06 Hz). **^{13}C NMR (100 MHz, DMSO-d_6) δ (ppm):** 144.4, 142.5, 129.8, 128.7, 126.4, 70.4, 70.3, 69.9, 69.6, 50.7, 35.2; MS (ESI positive) *m/z*: 549.3 $[M+H]^+$. Elemental analysis: calculated C, 45.97; H, 6.61; N, 15.32; found C, 45.98; H, 6.62; N, 15.33.

3.1.7. General procedure for the synthesis of compounds 10a-b, 11, 12a-c, 13, and 14b-d

Erlotinib hydrochloride (**ERL**) (1 equiv), sodium ascorbate (1.6 equiv), $CuSO_4$x$5H_2O$ (0.8 equiv) tetramethylammonium chloride (4.5 equiv) and the appropriate azide derivative **25a-b**, **26**, **28**, **29a-c**, or **32b-d** (1.1 equiv) were dissolved in H_2O/*tert*-butanol (1:1) and stirred overnight at 60 °C. Then, the reaction mixture was filtered through a cake of Celite 521© and the filtrate was treated with slush. The crude was extracted with EtOAc thrice. The combined organic layers were dried over anhydrous Na_2SO_4, filtered, and evaporated at reduced pressure. The crude material was purified by flash column chromatography (MeOH/DCM: 5:95), to yield compounds **10a-b**, **11**, **12a-c**, **13**, and **14b-d.**

1-(4-(3-((6,7-bis(2-methoxyethoxy)quinazolin-4-yl)amino)phenyl)-1*H*-1,2,3-triazol-1-yl)-*N*-(4-sulfamoylbenzyl)-3,6,9,12,15-pentaoxaoctadecan-18-amide (10a)

Yellow powder. Yield: 47%. **¹H NMR (400 MHz, DMSO-*d₆*) *δ* (ppm):** 9.55 (1H, s, N*H*, exchange with D₂O), 8.53 (1H, s), 8.48 (1H, s), 8.42 (1H, t, *J* = 5.90 Hz), 8.27 (1H, s), 7.93 (1H, s), 7.89 (1H, d, *J* = 9.02 Hz), 7.75 (2H, d, *J* = 7.98 Hz), 7.54 (1H, d, *J* = 7.63 Hz), 7.47 (1H, d, *J* = 8.06 Hz), 7.40 (2H, d, *J* = 8.29 Hz), 7.29 (2H, bs, SO₂N*H₂*, exchange with D₂O), 7.23 (1H, s), 4.58 (2H, t, *J* = 5.12 Hz), 4.30 (6H, m), 3.88 (2H, t, *J* = 5.12 Hz), 3.79 (2H, t, *J* = 4.44 Hz), 3.75 (2H, t, *J* = 4.44 Hz), 3.61 (2H, t, *J* = 6.15 Hz), 3.56 (2H, m), 3.50 (2H, m), 3.45 (14H, m), 3.38 (3H, s), 3.36 (3H, s), 2.38 (2H, t, *J* = 6.01 Hz). **¹³C NMR (100 MHz, DMSO-*d₆*) *δ* (ppm):** 170.8, 156.6, 153.9, 153.1, 148.4, 147.0, 146.4, 143.8, 142.5, 140.0, 131.2, 129.3, 127.5, 125.8, 122.0, 121.9, 120.6, 119.0, 109.1, 108.3, 103.5, 70.3, 70.2, 69.9, 69.8, 69.7, 68.8, 68.6, 68.3, 67.0, 58.6, 58.5, 49.8, 41.9, 41.8, 36.3; MS (ESI positive) *m*/*z*: 897.4 [M+H]⁺. Elemental analysis: calculated C, 52.34; H, 6.41; N, 13.56; found C, 52.33; H, 6.42; N, 13.55.

1-(4-(3-((6,7-bis(2-methoxyethoxy)quinazolin-4-yl)amino)phenyl)-1*H*-1,2,3-triazol-1-yl)-*N*-(4-sulfamoylphenethyl)-3,6,9,12,15-pentaoxanonadecan-19-amide (10b)

Green powder. Yield: 44%. **¹H NMR (400 MHz, DMSO-*d₆*) *δ* (ppm):** 9.58 (1H, s, N*H*, exchange with D₂O), 8.56 (1H, s), 8.51 (1H, s), 8.45 (1H, t, *J* = 5.90 Hz), 8.30 (1H, s), 7.96 (1H, s), 7.92 (1H, d, *J* = 9.02 Hz), 7.78 (2H, d, *J* = 7.98 Hz), 7.57 (1H, d, *J* = 7.63 Hz), 7.50 (1H, d, *J* = 8.06 Hz), 7.43 (2H, d, *J* = 8.29 Hz), 7.32 (2H, bs, SO₂N*H₂*, exchange with D₂O), 7.26 (1H, s), 4.61 (2H, t, *J* = 5.12 Hz), 4.33 (6H, m), 3.91 (2H, t, *J* = 5.12 Hz), 3.82 (2H, t, *J* = 4.44 Hz), 3.78 (2H, t, *J* = 4.44 Hz), 3.64 (2H, t, *J* = 6.15 Hz), 3.59 (2H, m), 3.53 (2H, m), 3.48 (16H, m), 3.41 (3H, s), 3.39 (3H, s), 2.41 (2H, t, *J* = 6.01 Hz). **¹³C NMR (100 MHz, DMSO-*d₆*) *δ* (ppm):** 175.9, 172.1, 157.4, 154.6, 153.7, 149.0, 147.0, 144.7, 142.0, 140.3, 131.5, 130.1, 130.0, 126.4, 123.0, 122.8, 121.6, 120.0, 109.6, 108.3, 103.8, 70.8, 70.7, 70.3, 70.2, 70.1, 69.2, 69.2, 68.9, 67.3, 62.7, 59.1, 56.1, 50.5, 49.3, 40.4, 36.7, 35.2; MS (ESI positive) *m*/*z*: 911.4 [M+H]⁺. Elemental analysis: calculated C, 54.21; H, 6.46; N, 13.00; found C, 54.20; H, 6.47; N, 13.01.

1-(4-(3-((6,7-bis(2-methoxyethoxy)quinazoline-4-yl)amino)phenyl)-1*H*-1,2,3-triazol-1-yl)-*N*-(2-((2-oxo-2*H*-chromen-6-yl)oxy)ethyl)-3,6,9,12,15-pentaoxaoctadecan-18-amide (11)

Green oil. Yield: 45%. **¹H NMR (400 MHz, DMSO-*d₆*) *δ* (ppm):** 9.68 (1H, s, N*H*, exchange with D₂O), 8.54 (1H, s), 8.51 (1H, s), 8.26 (1H, s), 8.11 (1H, t, *J* = 4.93 Hz), 7.98 (1H, d, *J* = 9.42 Hz), 7.94 (1H, s), 7.87 (1H, d, *J* = 8.35 Hz), 7.56 (1H, d, *J* = 7.59 Hz), 7.46 (1H, t, *J* = 7.84 Hz), 7.32 (1H, d, *J* = 8.85 Hz), 7.27 (1H, d, *J* = 2.85 Hz), 7.23 (1H, s), 7.19 (1H, dd, *J* = 8.87 Hz, 9.27 Hz), 6.48 (1H, d, *J* = 9.50 Hz), 4.58 (2H, t, *J* = 5.51 Hz), 4.30 (4H, m), 4.00 (2H, t, *J* = 5.55 Hz), 3.88 (2H, t, *J* = 5.10 Hz), 3.79 (2H, t, *J* = 4.80 Hz), 3.75 (2H, t, *J* = 4.35 Hz), 3.57 (4H, m), 3.49 (2H, m), 3.42 (12H, m), 3.37 (8H, m), 2.32 (2H, t, *J* = 6.37 Hz). **¹³C NMR (100 MHz, DMSO-*d₆*) *δ* (ppm):** 179.7, 170.4, 160.0, 156.5, 154.7, 153.8, 152.5, 148.2, 147.9, 146.1, 144.0, 139.7, 131.1, 129.0, 121.9, 121.8, 120.5, 119.8, 119.1, 118.9, 117.3, 116.5, 111.5, 108.9, 107.5, 103.4, 70.1, 70.0,

69.7, 69.6, 69.4, 68.6, 68.4, 68.1, 67.0, 66.7, 58.4, 58.3, 49.6, 47.2, 38.1, 36.0, 30.6; MS (ESI positive) m/z: 916.9 [M+H]$^+$. Elemental analysis: calculated C, 55.91; H, 6.41; N, 12.36; found C, 55.92; H, 6.42; N, 12.34.

3-(3-(17-(4-(3-((6,7-bis(2-methoxyethoxy)quinazoline-4-yl)amino)phenyl)-1H-1,2,3-triazol-1-yl)-3,6,9,12,15-pentaoxaheptadecyl)ureido)benzenesulfonamide (12a)

Yellow powder. Yield: 40%. **¹H NMR (400 MHz, DMSO-d_6) δ (ppm):** 9.56 (1H, s, NH, exchange with D$_2$O), 8.87 (1H, s, NH, exchange with D$_2$O), 8.53 (1H, s), 8.48 (1H, s), 8.27 (1H, s), 7.96 (1H, m), 7.93 (1H, s), 7.89 (1H, d, J = 8.71 Hz), 7.54 (1H, d, J = 7.87 Hz), 7.48 (2H, m), 7.34 (2H, m), 7.28 (2H, bs, SO$_2$NH_2, exchange with D$_2$O), 7.22 (1H, s), 6.23 (1H, t, J = 5.58 Hz), 4.58 (2H, t, J = 5.27 Hz), 4.30 (4H, m), 3.88 (2H, t, J = 4.96 Hz), 3.79 (2H, t, J = 4.34 Hz), 3.75 (2H, t, J = 4.23 Hz), 3.55 (2H, m), 3.46 (16H, m), 3.38 (3H, s), 3.36 (3H, s), 3.24 (2H, m). **¹³C NMR (100 MHz, DMSO-d_6) δ (ppm):** 156.4, 154.9, 153.6, 152.9, 148.1, 146.9, 146.2, 144.5, 140.9, 140.0, 131.0, 129.2, 128.9, 121.8, 121.7, 120.3, 120.2, 118.7, 118.0, 114.4, 109.0, 108.2, 103.3, 76.4, 72.9, 70.6, 70.1, 70.0, 69.7, 69.6, 68.6, 68.4, 68.0, 59.5, 58.4, 58.3, 56.6, 49.6, 47.2, 30.6; MS (ESI positive) m/z: 898.4 [M+H]$^+$. Elemental analysis: calculated C, 54.84; H, 6.17; N, 14.04; found C, 54.86; H, 6.15; N, 14.03.

4-(3-(17-(4-(3-((6,7-bis(2-methoxyethoxy)quinazolin-4-yl)amino)phenyl)-1H-1,2,3-triazol-1-yl)-3,6,9,12,15-pentaoxaheptadecyl)ureido)benzenesulfonamide (12b)

Reddish oil. Yield: 25%. **¹H NMR (400 MHz, DMSO-d_6) δ (ppm):** 9.59 (1H, s, NH, exchange with D$_2$O), 8.56 (1H, s, NH, exchange with D$_2$O), 8.50 (1H, s), 8.29 (1H, s), 7.95 (1H, s), 7.91 (1H, d, J = 8.23 Hz), 7.77 (2H, d, J = 7.84 Hz), 7.56 (1H, d, J = 8.07 Hz), 7.48 (1H, t, J = 7.81 Hz), 7.41 (2H, d, J = 8.22 Hz), 7.30 (2H, bs, SO$_2$NH_2, exchange with D$_2$O), 7.25 (1H, s), 6.54 (1H, t, J = 4.86 Hz), 6.05 (1H, t, J = 5.43 Hz), 4.61 (2H, t, J = 4.94 Hz), 4.32 (4H, m), 4.27 (2H, d, J = 5.87 Hz), 3.90 (2H, t, J = 5.10 Hz), 3.81 (2H, t, J = 4.34 Hz), 3.77 (2H, t, J = 3.06 Hz), 3.57 (2H, m), 3.47 (14H, m), 3.39 (8H, m). **¹³C NMR (100 MHz, DMSO-d_6) δ (ppm):** 158.3, 155.7, 154.9, 149.5, 148.6, 145.6, 143.7, 137.4, 135.9, 135.2, 131.4, 129.3, 126.7, 124.2, 123.1, 122.0, 121.3, 116.6, 107.2, 105.0, 100.6, 72.6, 69.9, 69.7, 69.6, 69.0, 68.8, 68.6, 58.4, 57.3, 51.3, 49.7, 44.0, 36.3, 35.4, 29.0; MS (ESI positive) m/z: 898.4 [M+H]$^+$. Elemental analysis: calculated C, 54.84; H, 6.17; N, 14.04; found C, 54.86; H, 6.16; N, 14.02.

4-(21-(4-(3-((6,7-bis(2-methoxyethoxy)quinazoline-4-yl)amino)phenyl)-1H-1,2,3-triazol-1-yl)-3-oxo-7,10,13,16,19-pentaoxa-2,4-diazahenicosyl)benzenesulfonamide (12c)

Yellow powder. Yield: 52%. **¹H NMR (400 MHz, DMSO-d_6) δ (ppm):** 9.57 (1H, s, NH, exchange with D$_2$O), 8.54 (1H, s, NH, exchange with D$_2$O), 8.48 (1H, s), 8.27 (1H, s), 7.93 (1H, s), 7.89 (1H, d, J = 8.23 Hz), 7.75 (2H, d, J = 7.84 Hz), 7.54 (1H, d, J = 8.07 Hz), 7.46 (1H, t, J = 7.81 Hz), 7.39 (2H, d, J = 8.22 Hz), 7.28 (2H, bs, SO$_2$NH_2, exchange with D$_2$O), 7.23 (1H, s), 6.52 (1H, t, J = 4.86 Hz), 6.03 (1H, t, J = 5.43 Hz), 4.59 (2H, t, J = 4.94 Hz), 4.30 (4H, m), 4.25 (2H, d, J = 5.87 Hz), 3.88 (2H, t, J = 5.10 Hz), 3.79 (2H, t, J = 4.34 Hz), 3.75 (2H, t, J = 3.06 Hz), 3.55 (2H, m), 3.45

(14H, m), 3.37 (8H, m), 3.15 (2H, m). **^{13}C NMR (100 MHz, DMSO-d_6) δ (ppm):** 162.6, 160.9, 158.3, 154.9, 152.8, 149.5, 146.9, 144.8, 140.1, 138.2, 135.2, 133.1, 129.3, 126.7, 124.2, 123.2, 122.1, 121.3, 116.6, 112.1, 108.7, 102.3, 98.2, 69.9, 69.7, 69.6, 69.0, 68.8, 68.6, 58.4, 57.3, 49.7, 44.0, 29.0; MS (ESI positive) m/z: 912.6 [M+H]$^+$. Elemental analysis: calculated C, 55.31; H, 6.30; N, 13.82; found C, 55.30; H, 6.31; N, 13.83.

1-(17-(4-(3-((6,7-bis(2-methoxyethoxy)quinazolin-4-yl)amino)phenyl)-1*H*-1,2,3-triazol-1-yl)-3,6,9,12,15-pentaoxa heptadecyl)-3-(2-oxo-2*H*-chromen-6-yl)urea (13)

White powder. Yield: 54%. **^{1}H NMR (400 MHz, DMSO-d_6) δ (ppm):** 9.56 (1H, s, N*H*, exchange with D$_2$O), 8.81 (1H, s, N*H*, exchange with D$_2$O), 8.53 (1H, s), 8.48 (1H, s), 8.27 (1H, s), 8.01 (1H, d, *J* = 9.6 Hz), 7.93 (1H, s), 7.89 (1H, d, *J* = 7.8 Hz), 7.79 (1H, d, *J* = 2.5 Hz), 7.54 (1H, d, *J* = 7.6 Hz), 7.49 (1H, dd, *J* = 9.2 Hz, *J* = 2.7 Hz), 7.45 (1H, t, *J* = 7.9 Hz) 7.27 (1H, d, *J* = 8.9 Hz), 7.22 (1H, s), 6.43 (1H, d, *J* = 9.5 Hz), 6.28 (1H, t, *J* = 5.4 Hz), 4.58 (2H, t, *J* = 4.9 Hz), 4.30 (4H, m), 3.88 (2H, t, *J* = 5.0 Hz), 3.79 (2H, t, *J* = 4.7 Hz), 3.75 (2H, t, *J* = 4.5 Hz), 3.55 (2H, m), 3.46 (16H, m), 3.37 (3H, s), 3.36 (3H, s), 3.23 (2H, m). **^{13}C NMR (100 MHz, DMSO-d_6) δ (ppm):** 179.7, 170.4, 160.0, 156.5, 154.7, 153.8, 152.5, 148.2, 147.9, 146.1, 144.0, 139.7, 131.1, 129.0, 121.9, 121.8, 120.5, 119.8, 119.1, 118.9, 117.3, 116.5, 111.5, 108.9, 107.5, 103.4, 70.1, 70.0, 69.7, 69.6, 69.4, 68.6, 68.4, 68.1, 67.0, 66.7, 58.4, 58.3, 49.6, 38.1, 36.0; MS (ESI positive) m/z: 887.6 [M+H]$^+$. Elemental analysis: calculated C, 59.58; H, 6.14; N, 12.63; found C, 59.56; H, 6.15; N, 12.64.

4-(3-(17-(4-(3-((6,7-bis(2-methoxyethoxy)quinazolin-4-yl)amino)phenyl)-1*H*-1,2,3-triazol-1-yl)-3,6,9,12,15-pentaoxaheptadecyl)thioureido)benzenesulfonamide (14b)

Yellow powder. Yield: 36%. **^{1}H NMR (400 MHz, DMSO-d_6) δ (ppm):** 9.95 (1H, s, N*H*, exchange with D$_2$O), 8.55 (1H, s, N*H*, exchange with D$_2$O), 8.49 (1H, s), 8.28 (1H, s), 7.94 (1H, s), 7.90 (1H, d, *J* = 8.23 Hz), 7.76 (2H, d, *J* = 7.84 Hz), 7.55 (1H, d, *J* = 8.07 Hz), 7.47 (1H, t, *J* = 7.81 Hz), 7.40 (2H, d, *J* = 8.22 Hz), 7.29 (2H, bs, SO$_2$N*H$_2$*, exchange with D$_2$O), 7.24 (1H, s), 6.53 (1H, t, *J* = 4.86 Hz), 6.04 (1H, t, *J* = 5.43 Hz), 4.60 (2H, t, *J* = 4.94 Hz), 4.31 (4H, m), 4.26 (2H, d, *J* = 5.87 Hz), 3.89 (2H, t, *J* = 5.10 Hz), 3.80 (2H, t, *J* = 4.34 Hz), 3.76 (2H, t, *J* = 3.06 Hz), 3.56 (2H, m), 3.47 (14H, m), 3.39 (8H, m). **^{13}C NMR (100 MHz, DMSO-d_6) δ (ppm):** 162.9, 148.8, 147.3, 146.5, 144.3, 141.9, 140.0, 138.9, 131.3, 129.5, 129.4, 128.4, 126.0, 125.9, 125.7, 122.1, 120.8, 119.2, 117.6, 112.1, 104.5, 70.3, 70.2, 69.9, 68.8, 68.7, 68.5, 60.3, 58.6, 56.5, 55.4, 49.9 48.7, 36.0, 29.1, 28.8, 22.2; MS (ESI positive) m/z: 914.4 [M+H]$^+$. Elemental analysis: calculated C, 53.87; H, 6.07; N, 13.79; found C, 53.85; H, 6.06; N, 13.78.

4-(21-(4-(3-((6,7-bis(2-methoxyethoxy)quinazoline-4-yl)amino)phenyl)-1*H*-1,2,3-triazol-1-yl)-3-thioxo-7,10,13,16,19-pentaoxa-2,4-diazahenicosyl)benzenesulfonamide (14c)

Yellow powder. Yield: 41%. **^{1}H NMR (400 MHz, DMSO-d_6) δ (ppm):** 10.15 (1H, s, N*H*, exchange with D$_2$O), 8.59 (1H, s, N*H*, exchange with D$_2$O), 8.53 (1H, s), 8.32 (1H, s), 7.98 (1H, s), 7.94 (1H, d, *J* = 8.23 Hz), 7.80 (2H, d, *J* = 7.84 Hz), 7.59 (1H, d, *J* = 8.07 Hz), 7.51 (1H, t, *J* = 7.81 Hz), 7.44 (2H, d, *J* = 8.22 Hz), 7.33 (2H, bs, SO$_2$N*H$_2$*, exchange with D$_2$O), 7.28 (1H, s), 6.57 (1H, t, *J* = 4.86

Hz), 6.08 (1H, t, *J* = 5.43 Hz), 4.64 (2H, t, *J* = 4.94 Hz), 4.35 (4H, m), 4.30 (2H, d, *J* = 5.87 Hz), 3.93 (2H, t, *J* = 5.10 Hz), 3.84 (2H, t, *J* = 4.34 Hz), 3.80 (2H, t, *J* = 3.06 Hz), 3.60 (2H, m), 3.50 (14H, m), 3.42 (8H, m), 3.20 (2H, m). **^{13}C NMR (100 MHz, DMSO-*d*$_6$) *δ* (ppm):** 155.4, 148.8, 146.5, 145.1, 144.3, 141.8, 140.0, 133.0, 131.3, 129.6, 129.3, 128.5, 126.0, 125.9, 125.7, 122.1, 120.8, 119.1, 115.8, 112.0, 104.5, 70.4, 70.3, 69.9, 68.8, 68.7, 68.4, 66.4, 61.9, 60.3, 58.6, 49.9, 48.7, 36.0, 29.1, 28.8, 22.3; MS (ESI positive) *m/z*: 928.4 [M+H]$^+$. Elemental analysis: calculated C, 54.35; H, 6.19; N, 13.58; found C, 54.32; H, 6.21; N, 13.56.

4-(22-(4-(3-((6,7-bis(2-methoxyethoxy)quinazolin-4-yl)amino)phenyl)-1*H*-1,2,3-triazol-1-yl)-4-thioxo-8,11,14,17,20-pentaoxa-3,5-diazadocosyl)benzenesulfonamide (14d)

Yellow powder. Yield: 42%. **^{1}H NMR (400 MHz, DMSO-*d*$_6$) *δ* (ppm):** 9.84 (1H, s, N*H*, exchange with D$_2$O), 8.52 (1H, s, N*H*, exchange with D$_2$O), 8.46 (1H, s), 8.25 (1H, s), 7.91 (1H, s), 7.87 (1H, d, *J* = 8.23 Hz), 7.73 (2H, d, *J* = 7.84 Hz), 7.52 (1H, d, *J* = 8.07 Hz), 7.44 (1H, t, *J* = 7.81 Hz), 7.37 (2H, d, *J* = 8.22 Hz), 7.26 (2H, bs, SO$_2$N*H*$_2$, exchange with D$_2$O), 7.21 (1H, s), 6.50 (1H, t, *J* = 4.86 Hz), 6.01 (1H, t, *J* = 5.43 Hz), 4.57 (2H, t, *J* = 4.94 Hz), 4.28 (4H, m), 4.23 (2H, d, *J* = 5.87 Hz), 3.86 (2H, t, *J* = 5.10 Hz), 3.77 (2H, t, *J* = 4.34 Hz), 3.73 (2H, t, *J* = 3.06 Hz), 3.54 (2H, m), 3.45 (14H, m), 3.35 (8H, m), 3.13 (2H, m), 2.97 (2H, m). **^{13}C NMR (100 MHz, DMSO-*d*$_6$) *δ* (ppm):** 153.3, 148.8, 145.2, 144.3, 141.9, 140.0, 138.3, 131.3, 129.7, 129.5, 129.4, 128.4, 125.9, 125.7, 122.1, 120.8, 119.2, 119.2, 112.1, 111.0, 104.3, 72.8, 70.3, 70.2, 70.1, 69.9, 68.8, 68.7, 68.5, 60.3, 58.6, 52.0, 49.9, 48.7, 36.0, 29.1, 28.8, 22.2; MS (ESI positive) *m/z*: 942.2 [M+H]$^+$. Elemental analysis: calculated C, 54.82; H, 6.31; N, 13.38; found C, 54.81; H, 6.33; N, 13.36.

2.1.6. Procedure for the synthesis of compound 1-(17-azido-3,6,9,12,15-pentaoxaheptadecyl)-3-(2-oxo-2H-chromen-6-yl)urea (25)

The appropriate coumarin **28**[110] (1 equiv) and the commercial 17-azido-3,6,9,12,15-pentaoxaheptadecan-1-amine **27** (1.1 equiv) were dissolved in ACN (10 mL) and the reaction mixture was stirred at reflux temperature overnight. Then, the reaction mixture was treated with slush and extracted with EtOAc thrice. The combined organic layers were dried over anhydrous Na$_2$SO$_4$, filtered, and evaporated at reduced pressure. The crude material was purified by flash column chromatography (MeOH/DCM: 2:98), to yield compound **25**. Brownish oil, Yield: 47%. **^{1}H NMR (400 MHz, DMSO-*d*$_6$) *δ* (ppm):** 8.81 (1H, s, N*H*, exchange with D$_2$O), 8.07 (1H, d, *J* = 9.9 Hz), 7.85 (1H, s, N*H*, exchange with D$_2$O), 7.54 (1H, d, *J* = 8.7 Hz), 7.33 (1H, d, *J* = 9.0 Hz), 6.49 (1H, d, *J* = 8.9 Hz), 6.29 (1H, t, *J* = 4.9 Hz), 3.57 (21H, m), 3.30 (3H, m). MS (ESI positive) *m/z*: 494.2 [M+H]$^+$. Elemental analysis: calculated C, 53.54; H, 6.33; N, 14.19; found C, 53.52; H, 6.32; N, 14.18.

2.2. Pan Assays Interference Compounds

The behaviour of final compounds as pan-assay interference compounds (PAINS)[111] was evaluated through two different web tools SwissADME (http://www.swissadme.ch, accessed 2024−01-07)[112] and False Positive Remover (https://www.cbligand.org/ PAINS/login.php,

accessed 2024−01−07).[113] JChem for Office (21.15.704, 2023) by ChemAxon http://www.chemaxon.com) was used for structure management, SMILES generation, and file conversion. All the analyzed compounds were "accepted" by both the web services.

2.3. In vitro carbonic anhydrase inhibition assay

The CA-catalyzed CO_2 hydration activity measurement was performed on an Applied Photophysics stopped-flow instrument using phenol red, at a concentration of 0.2 mM, as a pH indicator with 20 mM HEPES (pH 7.5) as the buffer, 20 mM Na_2SO_4, and following the initial rates of the CA-catalyzed CO_2 hydration reaction for a period of 10–100 s and working at the maximum absorbance of 557 nm. The CO_2 concentrations ranged from 1.7 to 17 mM.[114] For each inhibitor, six traces of the initial 5−10% of the reaction have been used to determine the initial velocity. The uncatalyzed reaction rates were determined in the same manner and subtracted from the total observed rates. Stock solutions of inhibitor (0.1 mM) were prepared in distilled water, and dilutions up to 0.01 nM were prepared. Solutions containing inhibitor and enzyme were preincubated for 15 min at room temperature before assay to allow the formation of the E−I complex. The inhibition constants were obtained as non-linear least-squares protocols using PRISM 3 and are the mean from at least three different measurements. All CAs were recombinant ones and were obtained *in-house*.[115]

2.4. Molecular Docking

The two-dimensional structures of the compounds were generated using the Maestro module of the Schrödinger Life-Sciences Suite 2024–1 software.[116] The LigPrep utility was then employed to prepare the compounds to obtain the three-dimensional geometry and identify all possible tautomers and protonation states at pH 7.0 ± 0.4, as determined by Epik.[117] The sulfonamide group was considered as deprotonated to evaluate the interaction with zinc ion, but after observing no interaction (even considering the zinc constraint and the core constraint), the sulfonamide group was used as unprotonated. The crystal structures of hCA I, hCA II, hCA IX, hCA XI, and EGFR were retrieved from the Protein Data Bank (PDB ID: 6I0J, 3K34, 8Q1A, 5LL5, and 3W2S, respectively).[118–122]

Protein Preparation workflow was used to correct, optimize and minimize the crystal structures. Molecular docking analyses were performed using the Glide software. Each enclosing box grid was generated using the centroid of the proper crystallographic ligand and the generated grid file was used for molecular docking using the SP-peptide module of Maestro.[123] In all CA isoforms, a water molecule was positioned in front of the zinc ion after no interaction between the zinc ion and the sulfonamide group was found. SP-peptide docking protocol was used by setting 5000 poses per ligand for the initial phase and 400 poses per ligand for energy minimization with the OPLS4 forcefield. The docking results were analyzed for the best-docked pose based on the Glide SP score.

### 2.5. *In vitro* cell proliferation assays

Human triple-negative breast cancer MDA-MB-231 cells (ATCC HTB-262) were cultured in Dulbecco's modified Eagle's medium (DMEM) with 10% fetal bovine serum (FBS), 1% penicillin/streptomycin, and 1% glutamine. Cells were kept at the low passage, returning to their original frozen stocks every 3–4 months. For hypoxic culture conditions cells were grown in 1% O_2 and 5% CO_2. Cell proliferation assays were performed seeding 10.000 cells/well in 48-well plates, and treatments were performed in 1% FBS with increasing concentrations of compounds **8b**-**d** and **7a**, **SLC-0111**, or **ERL**. After 72 h of incubation at 37 °C, cells detached using trypsin/2 mM EDTA, and cell counting was performed with a MACSQuant® Analyzer (Miltenyi Biotec).

3. RESULTS AND DISCUSSION

3.1. Synthetic approach

We recently reported the click chemistry approach applied to the hybridization of **ERL**, as an innovative strategy to tackle infections promoted by *Helicobacter pylori.* [64] Specifically, the hybrids obtained accounted for the **ERL** linked to the prototypic CA-inhibiting chemotype [65] (compounds **1-4**, **Figure 1**, **Table 1**) and for the pyrimidine-2,4(1*H*,3*H*)-dione moiety as in the antiviral azidothymidine (**AZT**) drug (namely **5**, **Figure 1**, **Table 1**) which is also endowed with antimicrobial features.[66,67]
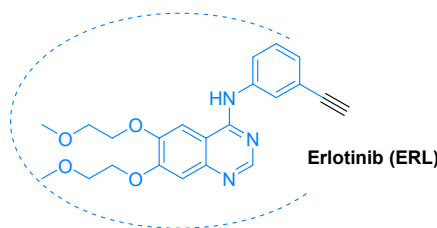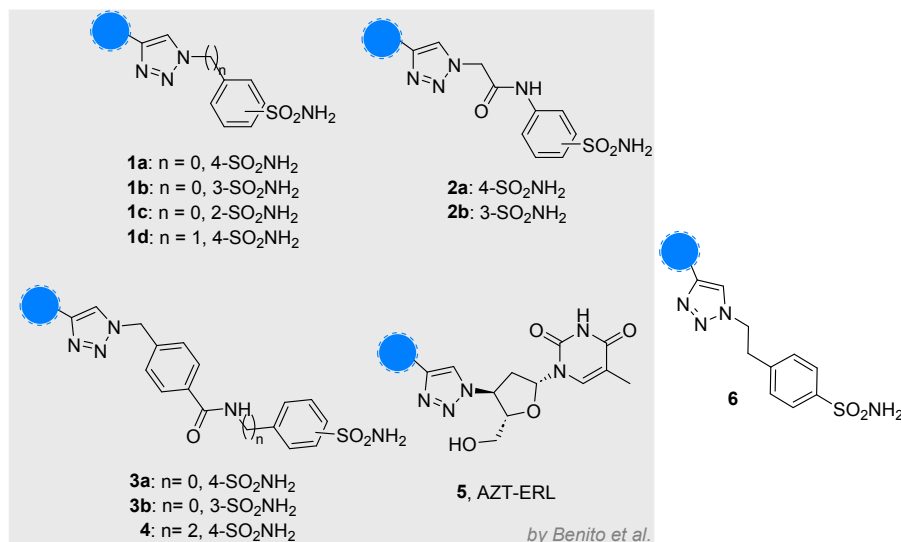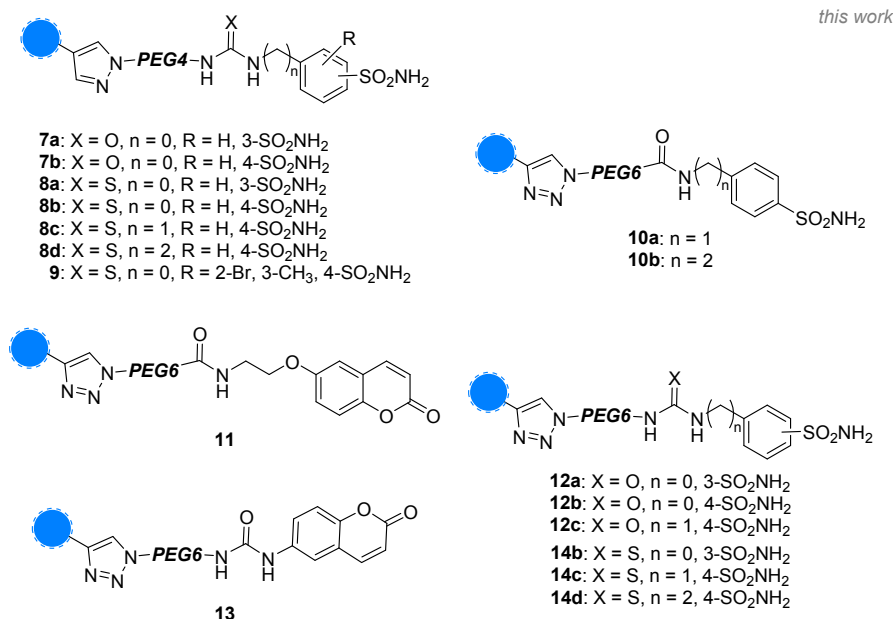
Figure 1. Structures of **ERL** and clicked derivatives from the 1st (**1-6**) and 2nd (pegylated **7-14**) series.

The main structural features contained in **1-5** were thought to inhibit the pathogenic expressed CA (HpαCA) which is fundamental for the microorganism survival at the harsh stomach pH values,[68,69] and to induce overexpression of EGFR in the host cells[70,71] along with its inhibition by the ERL portion.
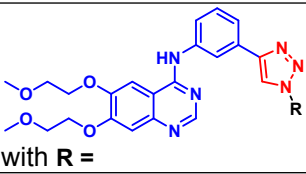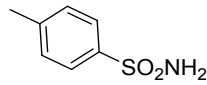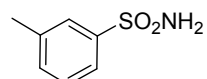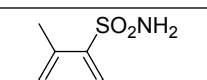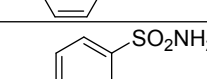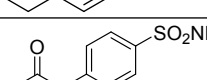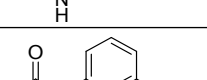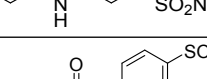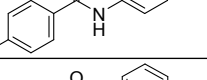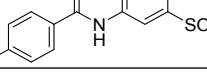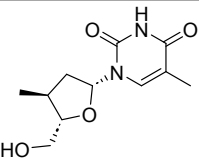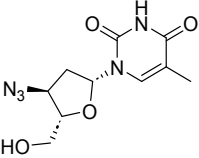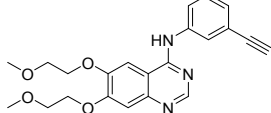
The synthesized compounds allowed us to define the tolerance of introduced modifications, thus including a preliminary exploration on spacers connecting the two active portions. The enzymatic results on a panel of bacterial CAs were highly promising, highlighting some compounds to potently and selectively inhibit HpαCA (**Table 1**) over other bacterial isoenzymes and exhibit a moderate anti-*H. pylori* activity, as shown by minimal bacterial concentration (MIC) values.[64] Interestingly, the emerged compound **2b** was also investigated *in silico* and the modification of the **ERL** structure into the triazole-containing tail was proved not to severely impair the binding to EGFR.[64]

Herein, as a follow-up of our research, this first series of **ERL**-clicked derivatives were tested on a selected panel of human (h) CAs such as the I, II, VA, VI, IX, and XII to assess their potency and selectivity profiles in comparison to **ERL** and **AZT** (**Table 1**).

Table 1. K_I values of **ERL**-clicked derivatives **1-5** and reference drug **AAZ**, **AZT**, and **ERL** on a panel of HpαCA and hCAs by means of stopped-flow hydration assay.[72]

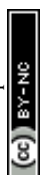| cpd	STRUCTURE	K_I (nM)						
	with R =	HpαCA*	hCA I*	hCA II*	hCA VA	hCA VI	hCA IX	hCA XII
1a		63.3	70.0	2.0	13.2	360	18.5	n.a.
1b		70.1	85.4	22.0	11.6	174	18.1	n.a.
1c		252	3503	5.0	n.a.	60.1	18.3	28.0
1d		19.3	9.3	4.5	13.0	51.3	20.0	6.0
2a		56.3	3.3	10.4	8.3	39.7	443	7.0
2b		71.6	382	7.4	12.4	99.0	393	n.a.
3a		48.0	35.2	5.4	98.0	2601	40.0	n.a.
3b		43.6	31.2	3.0	107	192	561	n.a.
4		805	2.6	5.0	6.2	28.1	425	n.a.
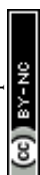
5		19.3	7.1	3.0	145	103	1445	n.a.
AZT		n.a.	n.a.	684	n.a.	505	n.a.	590
ERL		n.a.	n.a.	3976	n.a.	453	n.a.	n.a.
AAZ		21.0	250	12.1	63.0	16.0	25.7	5.7

K_I values are reported as means of three independent experiments. Errors are in the range of ± 5-10% of the reported values. **AAZ** was used as a reference control in these assays. n.a.: not active at the highest concentration tested (100 μM). Data on HpαCA and hCAs I and II (indicated with an asterisk, *) are already reported by Benito *et al.*[64]

Based on data in **Table 1** relevant structure-activity relationships (SARs) can be drawn. The presence of the 4-benzenesulfonamide group (**1a**) seems to be responsible for a selective inhibitory profile for hCA II (K_I = 2.0 nM), whereas a low nanomolar inhibition was also detected towards hCA VA and hCA IX (K_I values of 13.2 and 18.5 nM, respectively) (Selectivity Index (SI) values for the tumor-associated hCAs are reported in **Table S1** in the ESI file). Interestingly, no activity was found against the XII isoform. By moving the sulfonamide function in the meta-position of the phenyl ring, as in compound **1b**, the potency towards isoforms VA and IX was maintained (K_I values of 11.6 and 18.1 nM, respectively), with no significant difference, such as the lack of activity against hCA XII. Similar activities were also found on HpαCA and hCA I, whereas an 11-fold decrease in potency was noticed versus hCA II (K_I values of 22.0 nM) and a 2-fold lower K_I on hCA VI (= 360 and 174 nM for **1a** and **1b**, respectively). On the other hand, the ortho-isomer **1c** showed a very different inhibitory profile. In fact, the compound proved to be highly selective for hCA II, with a low nanomolar inhibition (K_I = 5.0 nM), and still maintained the potency against hCA IX (K_I = 18.3 nM). However, **1c** reverted the trend against the isoforms VA and XII; indeed, the complete loss of activity towards the former corresponded to a relevant gain in potency on hCA XII (K_I = 28.0 nM). Thereby, data for **1a-c** highlighted that the position of the zinc-binding group is not relevant in the inhibition of hCA IX, but fundamental to discriminate potency towards hCAs VA and XII.

A dramatic change was observed by introducing a methylene unit between the triazole ring and the para-benzenesulfonamide ring, as in compound **1d**: a net increase in the inhibitory potency is highlighted and low nanomolar K_I values were found for HpαCA, hCA I, hCA VI and hCA XII (=

RSC Medicinal Chemistry Accepted Manuscript

19.3, 9.3, 51.3, and 6.0 nM), although the potency against the isoforms II, VA, and IX were not relevantly affected with respect to **1a**. Introducing an amido moiety between the methylene unit and the benzenesulfonamide group in **2a** the inhibition of hCA XII was maintained (K_I = 7.0 nM), while resulting in a 2.9- and 22-fold weaker inhibitor of hCAs II and IX (K_I = 56.3 and 443 nM), respectively. Shifting the sulfonamide function in meta-position leading to compound **2b** resulted in a complete loss of activity towards hCA XII along with a general decrease in potency with the maximum example in the 115-fold reduced inhibition of hCA I (K_I = 382 nM), whereas the chemical modification was better tolerated by hCA II and hCA IX. The affinity towards the hCA XII active site was clearly reset by an additional structural complication, *i.e.,* the insertion of a benzyl group in the tail, resulting in distancing the **ERL** core from the CA inhibiting function, as in **3a** and **3b**. Also, inhibition of hCA II was quite unaffected (K_I values of 5.4 and 3.0 nM), whereas higher discrepancy was highlighted by enzymatic data on hCA VI (K_I = 2601 and 192 nM for **3a** and **3b**, respectively) and hCA IX (K_I = 40.0 and 561 nM for **3a** and **3b**, respectively). Surprisingly, despite the isomerism, the compounds shared a similar inhibitory profile against HpαCA and hCAs I, II, and VA. Additional tail elongation as in compound **4** severely worsened the K_I value till the submicromolar range (= 805 nM) against HpαCA, while improving the potency against hCAs I, II, VA, and VI. As regards the tumor-associated hCAs IX and XII, while for the former a K_I of 425 nM was detected, inactivity emerged for the latter. In the end, when the hybrid **5** was tested on hCAs IX and XII, again no worthy-of-note inhibition can be highlighted. Moreover, CA inhibition profiling of **AZT** and **ERL** did not provide satisfactory results.

The dataset for this series of compounds highlighted that the shorter the linker the higher the inhibitory potency towards the tumor-associated hCAs, with **1a-d** being the most active on hCA IX. Thus, the introduction of additional moieties (amido groups as in **2a** and **2b**) and/or hydrophobic portions (phenyl rings as in **2a**, **2b**, and **4**) in the spacer seemed to cause a loss in activity. However, we tried to slightly increase the linker without implementing the chemical complexity, thereby designing compound **6**, being a homologue compound that bears only a methylene unit more (**Table 2**, synthesis in **Scheme S1** in the ESI file).

Table 2. K_I values of **ERL**-clicked derivative **6** and homologues **1a** and **1d** on hCAs I, II, IX, and XII and related SIs by means of stopped-flow hydration assay.

cpd	STRUCTURE	K_I (nM)				SI			
		hCA I	hCA II	hCA IX	hCA XII	*I/IX*	*II/IX*	*I/XII*	*II/XII*
1a		63.3*	70.0*	18.5	n.a.	3.42	3.78	-	-
1d		19.3*	9.3*	20.0	6.0	0.96	0.47	3.21	1.55

6		1031	18.4	9.3	353	111	1.98	2.92	0.05

K_I values are reported as means of three independent experiments. Errors are in the range of ± 5-10% of the reported values. **AAZ** was used as a reference control in these assays. n.a.: not active at the highest concentration tested (100 µM). Data indicated with an asterisk (*) were already reported by Benito *et al.*[64] SI values are calculated as the ratio between the K_I values of the physiologically relevant CA isoform I or II (as indicated) and the CA isoform of interest (hCA IX or hCA XII, as indicated). The higher the SI value, the higher the isoform preference.

Data in **Table 2** showed compound **6** being a weak inhibitor of hCA I, with a micromolar inhibitory potency versus this isoenzyme (K_I = 1031 nM), and possesses a stronger affinity towards hCAs II and IX, showing K_I values of 18.4 and 9.3 nM, respectively. Interestingly, the compound exhibited a higher preference for hCA IX with respect to its homologues **1a** and **1d**, as highlighted by the SI values. However, the activity towards hCA XII decreased reaching the medium nanomolar range (K_I = 353 nM), also impacting the SI.

However, representative compounds of the **ERL**-clicked series (**1a-c**) were selected along with the reference hCAs IX and XII inhibitor **SLC-0111**, and **ERL** to evaluate their anti-proliferative effect *in vitro* on non-small cell lung carcinoma A549 and pancreatic epithelioid carcinoma PANC-1 cell lines, both characterized by overexpression of the tumor-associated hCA IX [73,74] and EGFR [75,76] (**Figure S1** in the ESI file). The reference compound **SLC-0111** was found to be ineffective in reducing the proliferation of both the cell lines and only **ERL** and compound **1c** displayed an antiproliferative effect, with the latter being the most effective and possessing IC_{50} values of 16.3 and 57.1 µM on A549 and PANC-1 cells, respectively.

The overall promising results encouraged further investigation and the design of a second series of hybrids aimed at enhancing the compounds solubility. Thereby, in place of the traditional methylene chains,[20,77] we introduced non-cleavable monodispersed poly(ethylene glycol) (PEG) spacers between the pharmacophores interacting with hCAs and EGFR. Thus, we selected 4- and 6-unit PEG spacers to hold a precise length and good flexibility, which should ensure the two active portions could better fit into their targeted binding sites. In fact, due to their non-toxicity and amphiphilic nature, PEG polymers have garnered attention in pharmaceutical technologies, being included in formulations as excipients or vehicles/carriers of small molecules, biopharmaceuticals (*e.g.*, peptides, antibody-drug conjugates), and drug delivery systems (*e.g.,* liposomes and nanoparticles) or covalently bound to the drug of interest.[78] In this case, PEGylated biopharmaceuticals[79] and small molecule drugs[80] resulted in decreased immunogenicity and improved half-life in blood and showed increased metabolic stability, solubility, and overall enhanced pharmacokinetic properties. Known examples are the FDA-approved PEGylated naloxegol,[81] PEG-docetaxel,[82] PEG-camptothecin,[83] and many others.[84] However, few

small molecules-based hybrid compounds have been reported to possess PEG spacer[85] with respect to the widely explored PROTACs[86] and antibody-drug conjugates.[87]

Thus, we generated seventeen new compounds as Pegylated **ERL**-CAI hybrids (**7-14**, **Figure 1**) through the Huisgen click chemistry reaction. After synthesis, the compounds were then tested on hCAs I and II along with the tumor-associated isoforms IX and XII, and docking simulations helped the rationalization of the enzymatic results, and the affinity towards EGFR was investigated *in silico*. In the end, to assess the compounds antiproliferative effect, we moved towards the triple-negative breast cancer (TNBC) cell line MDA-MB-231, characterized by the upregulation of both EGFR and the tumor-associated hCAs.[88]

3.2. Synthesis of the ERL-based library

The synthetic pattern aimed at introducing PEG (= 4 or 6 oxyethylene units) spacers between the CA-interacting functionalities, such as benzenesulfonamide and coumarin, and **ERL**. The first series of derivatives (**7-9**) was successfully obtained by a two-step procedure involving the insertion of the PEG-4 linker by means of the nucleophilic attack of the amino head of **15** to the electrophilic carbamates **16a-b** or isothiocyanates **17a-d** and **18** on the benzenesulfonamide tails. The obtained intermediates **19a-b**, **20a-d**, and **21** were then reacted with **ERL** via a CuAAC by using nanosized copper in presence of tetramethylammonium chloride (TMACl) in DMF, affording the final compounds **7-9** (**Scheme 1**).
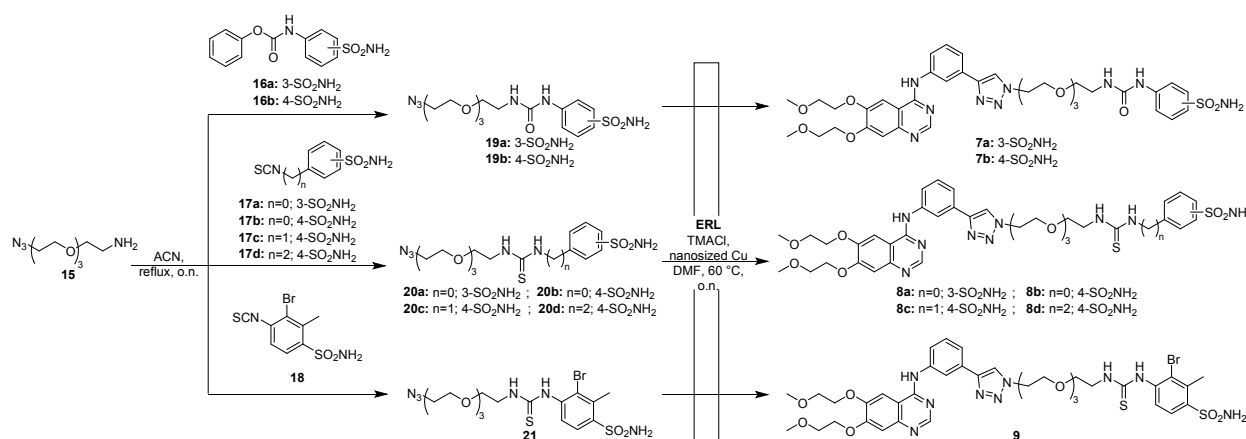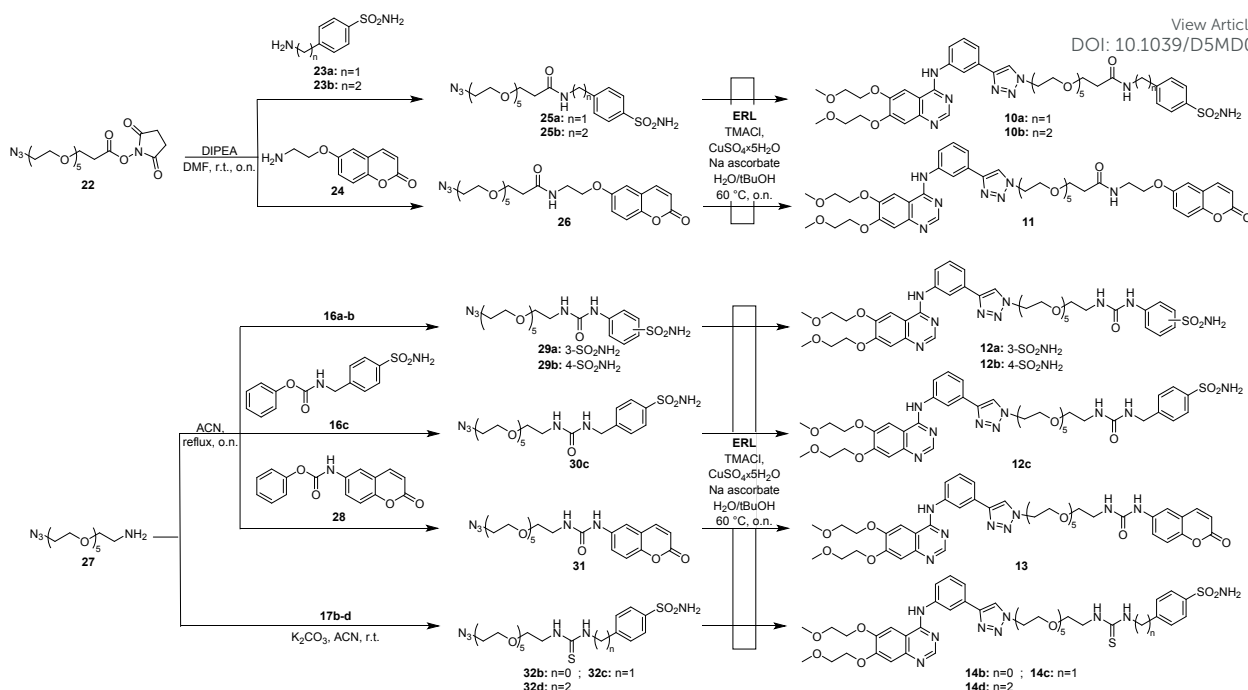

Scheme 1. Synthesis of hybrids **7-9**.

The second series of derivatives (**10-14**) was synthesized starting from the *N*-hydroxysuccinimide ester-functionalized PEG-6 (**22**) and suitable amines **23a-b** and **24**, gaining intermediates **25a-b** and **26**, tailored with benzenesulfonamide and coumarin cores, respectively (**Scheme 2**). Similarly, the amino group of the PEG-6 chemical **27** reacted with carbamates **16a-c** and **28** and thiocarbamates **17b-d** to obtain intermediates **29-32**. In the end, all the intermediates were clicked on **ERL** by using copper sulfate and sodium ascorbate in presence of TMACl, yielding the final compounds **10-14** (**Scheme 2**).
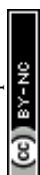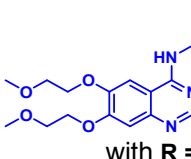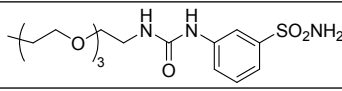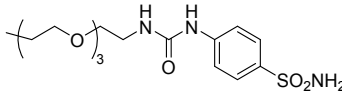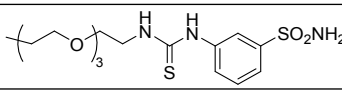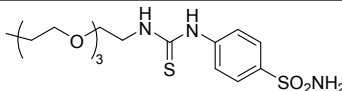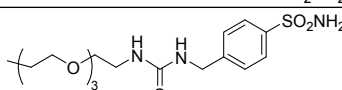
Scheme 2. Synthesis of hybrids **10-14**.
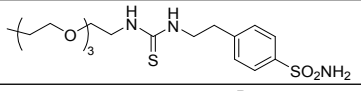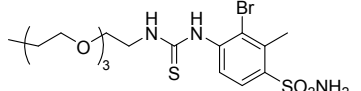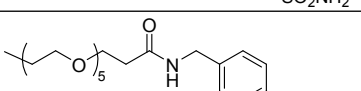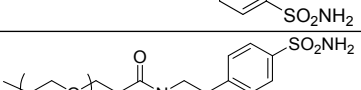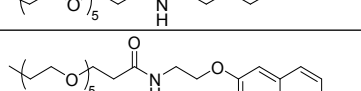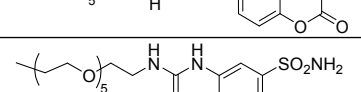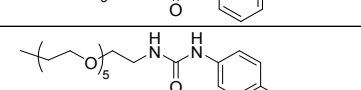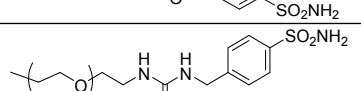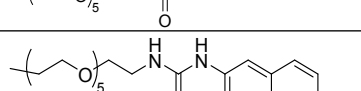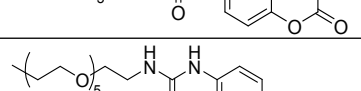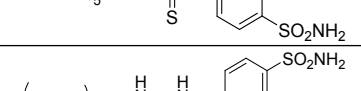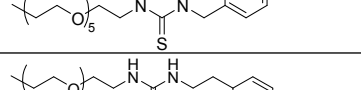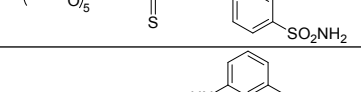
3.3. In vitro enzymatic inhibition on CAs

This library of **ERL**-derived compounds was tested for the capability to exert selective inhibition of a panel of four human CAs using the stopped-flow CO_2 hydration assay.[72] Data obtained were also compared with those of the reference AAZ and reported in **Table 3** as K_I values.

Table 3. K_I and SI values of **ERL**-clicked derivatives **7-14** and reference drugs **ERL** and **AAZ** versus a panel of hCAs and by means of stopped-flow hydration assay.[72]

cpd	STRUCTURE with R =	K_I (nM)				SI			
		hCA I	hCA II	hCA IX	hCA XII	I/IX	II/IX	I/XII	II/XII
7a		46546	723	285	58.9	164	2.54	790	12.3
7b		36052	950	1124	57.4	32.1	0.85	628	16.6
8a		45796	3169	1924	72	23.8	1.65	636	44.0
8b		3144	135	112	5.33	28	1.2	590	25.4
8c		3277	1150	26	69.7	127	44.57	47.0	16.5

RSC Medicinal Chemistry Accepted Manuscript

8d		923	106	28	6.49	32.6	3.73	142	16.3
9		4909	531.0	1345	69.8	3.65	0.39	70.3	7.61
10a		903	253	4158	3305	0.22	0.06	0.27	0.08
10b		632.4	33.5	3673	1363	0.17	0.01	0.46	0.02
11		70140	33700	4677	n.a.	15.0	7.21	-	-
12a		70090	1023	4473	6403	15.7	0.23	11.0	0.16
12b		24790	90.8	5620	75.3	4.41	0.02	329	1.21
12c		160	0.80	387	940	0.41	0.002	0.17	0.0008
13		28301	11364	242	8059	117	46.9	3.51	1.41
14b		43340	9712	4928	1523	8.79	1.97	28.4	6.38
14c		4976	1011	3727	665	1.33	0.27	7.48	1.52
14d		957	32703	1877	95.2	0.51	17.4	10.0	344
ERL		n.a.*	3976*	n.a.	n.a.	-	-	-	-
AZT		250	12.1	25.7	5.7	9.73	0.47	43.86	2.12

K_I values are reported as means of three independent experiments. Errors are in the range of ± 5-10% of the reported values. **AAZ** was used as a reference control in these assays. n.a.: not active at the highest concentration tested (100 µM). Data indicated with an asterisk (*) were already reported by Benito *et al.*[64] SI values are calculated as the ratio between the K_I values of the physiologically relevant CA isoform I or II (as indicated) and the CA isoform of interest (hCA IX or hCA XII, as indicated). The higher the SI value, the higher the isoform preference.

As reported in **Table 3**, interesting SARs for each CA isoform can be deduced.
i) As for the hCA I, all the derivatives are not strongly effective inhibitors, being the associated K_I values in the micromolar range (except for nanomolar inhibitors **8d**, **10a**, **10b**, **14d**, and above all **12c**). Compounds showed less potency when the PEG units are 6 (**10-14**), while the inhibitory
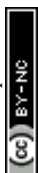
activity is improved with PEG-4 (**7-9**). The CA inhibiting warhead must be the benzenesulfonamide with respect to the coumarin ring (**11** and **13**). In the presence of PEG-4, thiourea is preferred over urea especially if not close to the $ArSO_2NH_2$ (n = 2 > 1 > 0). 3-SO_2NH_2 and 4-SO_2NH_2 contributed equally to the inhibitory activity. If the linker is PEG-6, thiourea is like urea especially if not close to the $ArSO_2NH_2$ (n = 2 > 1 > 0). The amide was a good option to substitute the (thio)urea moiety but only if n = 2 > 1.

ii) Overall, the kinetic trend for the hCA II is better for almost all the compounds (**23c** is even in the picomolar range K_I = 0.8 nM). Again, PEG-6 is preferred over PEG-4 and the CA inhibiting warhead must be the benzenesulfonamide with respect to the coumarin ring (**11** and **13**). If the linker is PEG-4, thiourea is more favored than urea, especially if n = 2 > 0 > 1. Conversely, if the linker is PEG-6, urea is better (n = 1 > 0 > 2) than thiourea, whereas the amide moiety can be a valid alternative.

iii) For hCA IX, the general situation is preferred for PEG-4. In this series, 4-SO_2NH_2 impacts positively the inhibitory values with respect to 3-SO_2NH_2, and thiourea and urea contributed equally (n = 1 ≥ 2 > 0). In the subset PEG-6, compounds are almost in the same micromolar range (except for **12** and **13**).

iv) The most interesting data were registered for hCA XII: if the linker is PEG-4 (better than 6), 4-NH_2SO_2Ar improves the inhibitory values with respect to 3-NH_2SO_2Ar and, again, thiourea is preferred to urea with n = 0-1 > 2. In the subset PEG-6, coumarins are still not important for the activity (high micromolar activity for compound **13** and no activity for compound **11**) and amide is more tolerated than (thio)urea especially if the 4-SO_2NH_2 moiety is present and with n = 2 > 0 > 1 in the thiourea series and n = 0 > 1 for ureas.

Isoform selectivity could be easily assessed by analyzing SI values reported in **Table 3**. Taking into consideration the first subset of PEG-4 derivatives (**7**-**9**), the higher affinity towards hCA XII was demonstrated by a large number of compounds with respect to isoforms I and II, with SI (I/XII) values ranging from 47.0 up to 790. Conversely, hCA IX inhibitory data almost overlapped with the values determined against hCA II in terms of potency range, not showing remarkable selectivity. However, the PEG-6 derivatives series (**10-14**) required a more accurate analysis of SI values since each compound seem to show a different isoform preference.

3.4. *In silico* studies on targeted enzymes

To rationalize the enzyme inhibition data, structure-based computational studies were conducted on all studied CA isoforms. The crystallographic structures of hCAs I, II, IX, and XII were obtained from the Protein Data Bank (PDB ID: 6I0J, 3K34, 8Q1A, and 5LL5, respectively). The selection of the PDB structures, validated in our previous works as well, was made taking into account the good crystallographic resolution and the absence of structural defects in the chosen structures. The investigation focused on compounds demonstrating the highest activity toward hCAs IX and

XII while exhibiting selectivity over hCAs I and II. Thereby, the *in silico* study included compounds **8b**, **8c**, and **8d** (**Table 3**).

Given their chemical structure, dimension, and flexibility, the Glide SP-peptide docking method was employed. In the initial trial, the sulfonamide group was assumed to be deprotonated in order to ascertain the potential for interaction with the zinc ion in the active site. This binding mode has not yet been observed in any X-ray crystal structure of CA-sulfonamide adducts[54] and should be checked experimentally in order to be validated. Unexpectedly, the docking poses obtained without any constraint do not exhibit the sulfonamide functionality of the compounds coordinated with the zinc ion. In some cases, the **ERL**-derived portion of the three compounds interacts with some residues in the active site. The protocol was then modified by introducing a constraint on the zinc ion, yet no poses in which this ion coordinates the sulfonamide were obtained. Subsequently, the core constraint approach was employed to force the sulfonamide group to coordinate the metal center, but the results were again negative. Because of the evidence that there is no direct interaction between the zinc ion and the sulfonamide group of compounds in this theoretical *in silico* approach, a coordination water molecule was introduced to the zinc ion in the hCA isoforms, with the sulfonamide group assumed to be in its undeprotonated form at physiological pH. The docking poses obtained with the docking SP-peptide were clustered, and the representative geometry of the most abundant cluster for each compound and each enzyme was considered. In hCA XII, compounds **8b** and **8d** (**Figure 2a-b**) are positioned outside the active site and form a cation-π interaction between Lys69 and the phenyl ring of the **ERL** fragment. Additionally, the sulfonamide NH_2 establishes two H-bonds with the carbonyl of the Gly169 backbone and the carbonyl oxygen of Glu171. In the case of **8d**, in addition to the H-bond between the amide nitrogen of Asn71 and the proximal oxygen of the 2-methoxyethoxy tail of **ERL**, the two nitrogen atoms of the thiourea directly linked to benzenesulfonamide mediate two H-bonds with Asn64.

The arrangement of compound **8c** (**Figure 2c**), which possesses 10 times less activity, differs from that of the other compounds. It enters the active site with the thiourea group, whose two nitrogen atoms mediate two H-bonds with the oxygen of Thr199. Additionally, the first oxygen atom of the ethoxy linker forms an H-bond with the nitrogen of Gln89. At the edge of the active site, the sulfonamide forms an H-bond with the amine group of Lys3, while H-bonds between the nitrogen of the triazole and Lys69 and between Leu60 and the oxygen of the **ERL** tail are observed outside the active site.
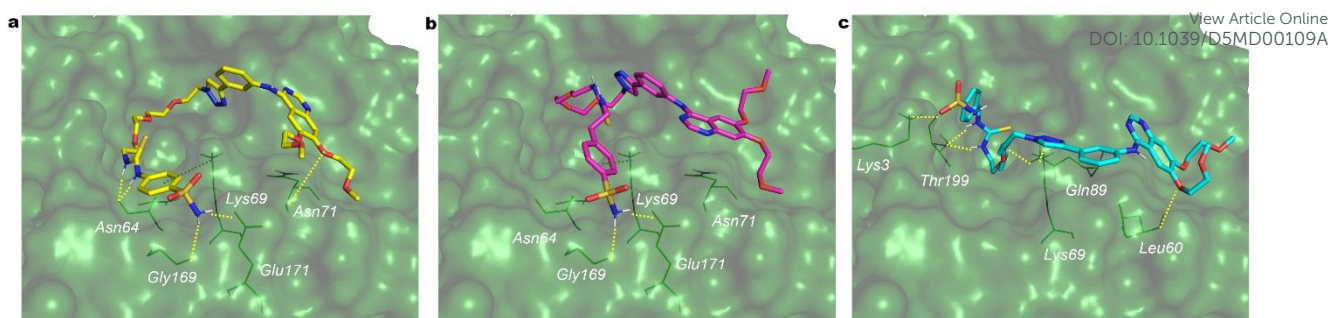
Figure 2. Predicted 3D binding mode within hCA XII (green surface) of compounds (a) **8b** (yellow sticks), (b) **8d** (magenta sticks), and (c) **8c** (cyan sticks). H-bond interacting residues are shown as green lines while H-bonding and cation-π interactions as yellow and green dotted lines, respectively.

Compounds **8c** and **8d** (**Figure 3b-c**), exhibiting a potent inhibition of hCA IX, gain access to the active site of hCA IX, despite their differing geometries. The sulfonamide moiety of **8b** or **8d** (**Figure 3a-b**) forms an H-bond with the zinc-coordinated water molecule, while the aromatic ring of **8d** engages in a π-π interaction with the zinc-coordinated His94. The nitrogen of the thiourea moiety of the three compounds forms an H-bond with His68.

In the region external to the active site, the quinazoline moiety of the **ERL** portion of **8c** (**Figure 3c**) engages in a cation-π interaction with Arg62, whereas the terminal methoxy of the 6-(2-methoxyethoxy) substituent of **8d** forms an H-bond with Arg89. Furthermore, two oxygen atoms of the PEG linker of **8d** form H-bonds with Arg64. As regards compound **8b**, no strong interactions are observed outside the active site.

Figure 3. Predicted 3D binding mode within hCA IX (pink surface) of compounds (a) **8b** (yellow sticks), (b) **8d** (magenta sticks), and (c) **8c** (cyan sticks). H-bond interacting residues are shown as magenta lines, while H-bonding, π-π interactions, and cation-π interactions as yellow, cyan, and green dotted lines, respectively.

All three compounds are positioned on the surface of hCA I without entering the active site, justifying the lack of activity toward this isoform. However, they display distinct binding modes within the hCA II isoform. Interestingly, **8c** remains outside the active site, exhibiting no evidence of bonding that could justify its observed activity. On the other hand, **8d** (**Figure 4b**) enters the active

site with the **ERL** moiety, and the two methoxy groups form H-bonds with Asn62 and Gln92. The triazole moiety engages in a π-π interaction with Phe131, the nitrogen atom of the thiourea moiety forms an H-bond with Asp130, whereas the nitrogen and oxygen atoms of the sulfonamide moiety form H-bonds with Asp72 and the backbone of Phe131, respectively. Conversely, **8b** (**Figure 4a**) enters the active site with the **ERL** portion, and the only notable interactions outside the active site are H-bonds between the triazole nitrogen and Trp5, and between the oxygen and nitrogen atoms belonging to the sulfonamide moiety and Arg58 and Gly171, respectively. Furthermore, a π-π interaction between the triazole and Phe20 can be observed.

In summary, compounds **8b**, **8c**, and **8d** were proven to establish favorable interactions within and outside the active site of the hCAs IX and XII isoforms, thereby justifying their observed activity and selectivity.
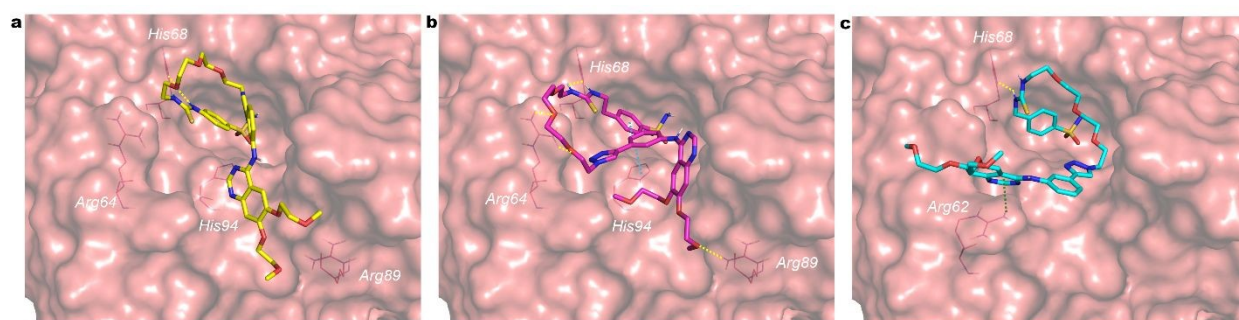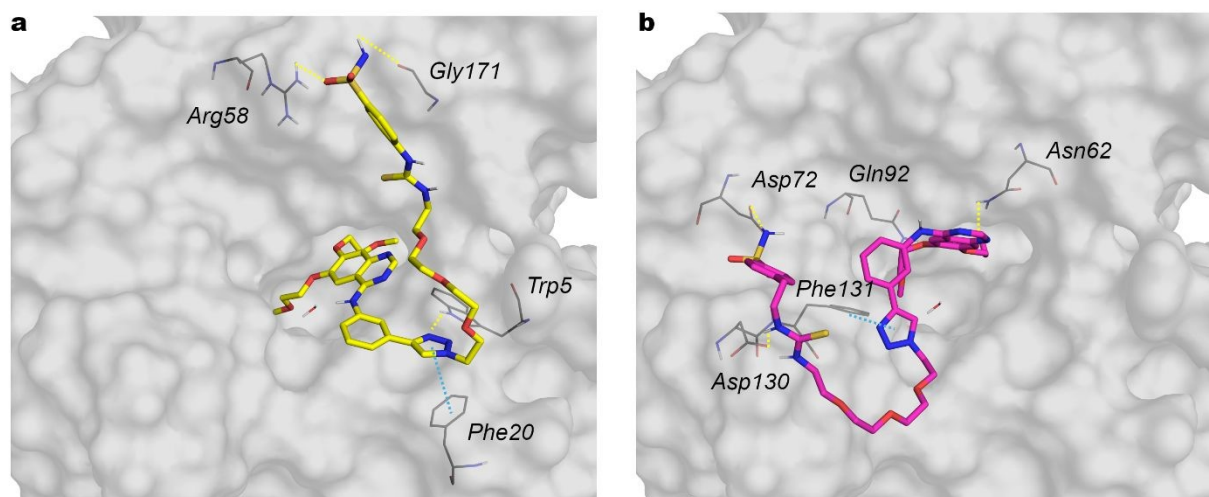

Figure 4. Predicted 3D binding mode within hCA II (grey surface) of compounds (a) **8b** (yellow sticks) and (b) **8d** (magenta sticks). H-bond interacting residues are shown as green lines while H-bonding and π-π interactions as yellow and cyan dotted lines, respectively.

Although the activity toward EGFR kinases has yet to be evaluated, we conducted a docking study on the EGFR kinase domain with the same compounds to evaluate a potential dual activity. Among the available protein in the Protein Data Bank, the PDB ID 3W2S was selected on the basis of the dimensions of the crystal ligand, which is comparable to those of compounds under investigation. The three compounds were observed to dock within the ATP binding site, forming hydrophobic interactions. Furthermore, compounds **8c** and **8d** (**Figure 5a-b**) establish H-bonds between the sulfonamide and Lys875 (**8c** with Val876), while **8b** interacts with Ala859. Lys745 forms an H-bond with the oxygen of the oxyethylene linker of **8d** and with two oxygens of **8c**. The aromatic ring of the benzenesulfonamide of **8c** forms a cation-π interaction with Arg841, while the nitrogen atoms of the thiourea of **8b** and **8d** engage in H bond interactions with Gly857 and Asp855, respectively. These observations are consistent with the docking score and conserved key interactions, which

indicate that **ERL** derivatives retain the structural features necessary for binding to the EGFR kinase domain.
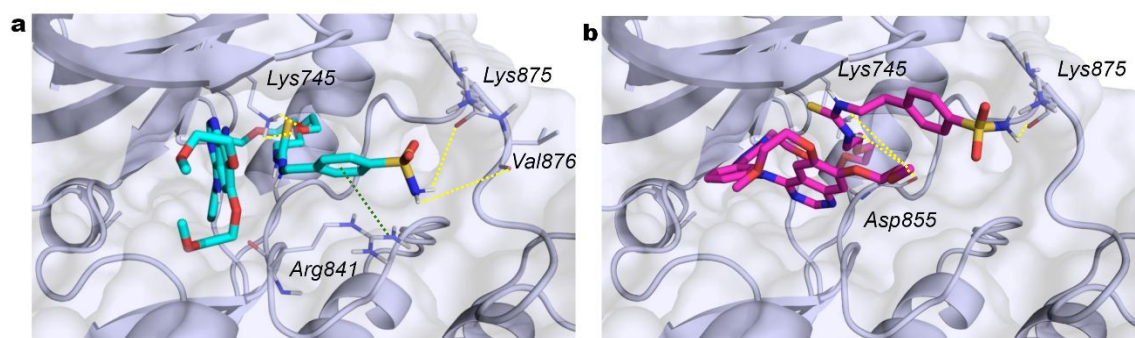
Figure 5. Predicted 3D binding mode within EGFR kinase domain (blue-grey surface and cartoon) of compounds (a) **8c** (cyan sticks) and (b) **8d** (magenta sticks). H-bond interacting residues are shown as grey lines while H-bonding and cation-π interactions as yellow and green dotted lines, respectively.

3.5. Anti-proliferative effect on TNBC cells

TNBC is one of the most reported causes of death in the female population worldwide[89] and one of its distinguishing features compared to other breast cancers is the overexpression of EGFR.[90–93] Interestingly, this receptor was proven to be activated in several TNBC cell lines[94,94] and its inhibition was demonstrated to arrest tumor growth and metastasis in TNBC xenograft models[95,96] by controlling the initial progression of the disease.[97] However, drug resistance to **ERL** has been recorded in some patients[98–100] with an unclear mechanism.[88] Also, **ERL** seems to inhibit the non-cancer stem cells, responsible for stemness and drug-resistance, or bulk TNBC cells.[101]

Thus, we selected representative compounds of the new series (**8b-d** and **7a**) to evaluate their anti-proliferative effect *in vitro* on the human TNBC cell line MDA-MB-231 that expresses both the tumor-associated hCA isoenzymes and EGFR.[60,102] We also tested the known hCAs IX and XII inhibitor **SLC-0111**, and **ERL**, as reference compounds (**Figure 6**). Cancer cells were treated with the compounds at increasing concentrations under hypoxic culture conditions, and the anti-proliferative readout was assessed after 72 hours by flow cytometry-based cell counting. As shown in **Figure 6**, the reference compound **SLC-0111** was found to be effective in reducing the proliferation of MDA-MB-231, with an IC_{50} of 23.4 μM. Interestingly, compounds **8b** and **8d** displayed the most promising anti-proliferative effect, with IC_{50} values ranging from 30 and 48.51 μM, respectively. A significantly lower effect on tumor cells was observed for compound **8c** (IC_{50} ~190 μM). Notably, treatment with **ERL** resulted only in a mild reduction of cell proliferation observed only at the higher 100 μM concentration tested, in accordance to our previous studies

underlining its lack of efficacy on this cell line,[101] thus supporting the increased effect obtained with the novel **ERL**-derived compounds.
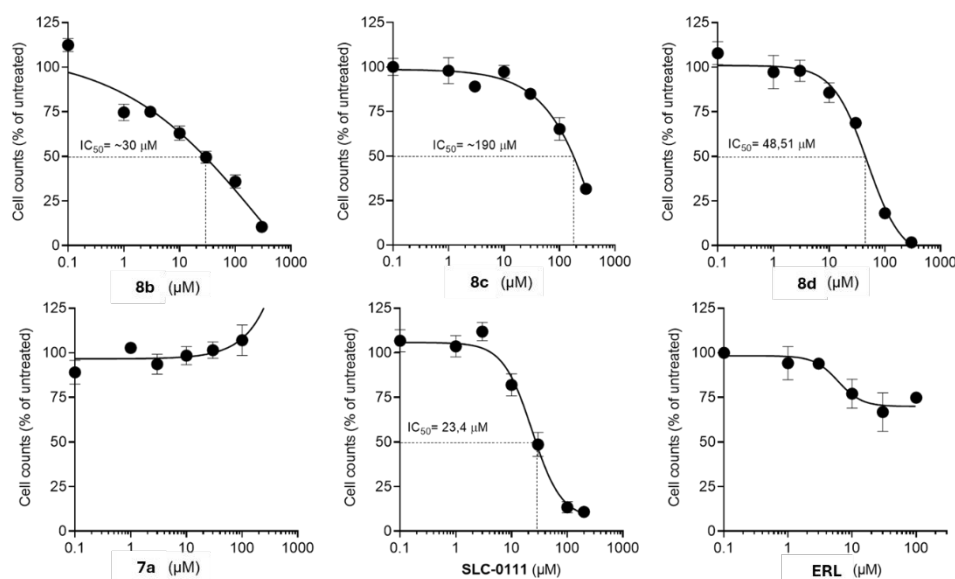
Figure 6. Cell proliferation of TNBC MDA-MB-231 cells treated for 72 hours in hypoxic conditions with compounds **8b**-**d** and **7a**, **SLC-0111**, or **ERL**. Cell count is referred to the untreated/control considered as 100%, mean ± SEM, and the IC_{50} are reported.

4. CONCLUSIONS

In summary, a second series of seventeen new Pegylated **ERL**-CAI hybrids was synthesized through the Huisgen click chemistry reaction, bearing the benzenesulfonamide or the coumarin moiety as pharmacophores. Two different linker lengths were selected, *i.e.* 4- and 6-unit PEG spacers, to hold good flexibility and simultaneously explore the best length for coordination with the zinc ion within the CA active cleft, thus enhancing pharmacokinetic properties. Most of the derivatives were found to strongly inhibit hCAs IX and XII at low-to-high nanomolar concentration, showing isoform selectivity in a large number of compounds. Concerning hCA IX the general situation shows a remarkable preference for PEG-4 derivatives. Moreover, no differences between thiourea and urea emerged, while the sulfonamide moiety position showed a high impact in K_I values ($4\text{-}SO_2NH_2 > 3\text{-}SO_2NH_2$). The same linker length preference is confirmed against hCA XII, in which the PEG-4 linker showed the best results. As well as previous isoform, thiourea is preferred to urea for hCA XII inhibition, with n = 0-1 > 2, and, similarly to hCA IX, $4\text{-}SO_2NH_2$ improved inhibitory features with respect to $3\text{-}SO_2NH_2$. Selectivity Index (SI) values were then used to assess isoform selectivity: Compounds **7-9** (PEG-4) showed a high preference for hCA XII (SI up to 790.25) compared to hCA I and II, while compounds **10-14** (PEG-6) had similar activity against hCA IX and II, with some selectivity over hCA I. The lower SI values (down to 345.52) for the latter group reflect their stronger inhibition of hCA IX and XII.

RSC Medicinal Chemistry Accepted Manuscript
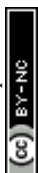
Computational molecular docking studies on hCA isoforms rationalize the inhibitory activity and selectivity of compounds **8b**, **8c**, and **8d**. Concerning hCA XII, **8b** and **8d** bind outside the active site, with key cation-π and hydrogen bonding interactions. Conversely, **8c** enters the active site differently. For hCA IX all three compounds showed binding within the active site, with the sulfonamide group of **8b** and **8d** forming an H-bond with a zinc-coordinated water molecule, and the aromatic ring of **8c** interacting with His94. Moreover, minimal interactions in the active sites of hCA I and II do support compounds' selectivity profile. Notably, docking study to the EGFR kinase domain indicated potential for dual activity. Thus, compounds **8b**, **8c**, and **8d** docked within the ATP binding site and retained key binding features, indicating the conservation of structural elements needed for binding to the EGFR domain, as well. We further evaluated new synthesized hybrids compounds for TNBC treatment, using the MDA-MB-231 cell line which expresses EGFR and hCAs. Compounds **8b** and **8d** demonstrated strong anti-proliferative activity (IC_{50} 30 and 48.51 µM respectively), thus comparable to the single target hCA inhibitor **SLC-0111** (IC_{50} = 23.4 µM) and in contrast to the low efficacy observed for the EGFR inhibitor **ERL**. These results highlight the potential of such compounds for further development within TNBC therapy and more.

Data availability

The data supporting this article have been included as part of the Supplementary Information. The following data are made available in the ESI:

Selectivity index (SI) values for the first ERL-clicked derivatives (Table S1); Synthesis of compound 6 (Scheme S1); Procedure for the synthesis of compound 6); Antiproliferative effect of the first series of ERL clicked derivatives (Figure S1); ^1H and ^{13}C NMR of representative compounds.

The ESI file contains the NMR spectra of the compounds reported in this article.

Authors Contribution (CREDIT)

Conceptualization, Review and Editing, S.C., I.D.A., A.A., F.C., and C.T.S.; Methodology and Formal Analysis, G.R., S.F., B.G., M.F., G.B., M.L.M., R.S., C.C., R.R.; Funding acquisition, F.C., R.R.; Writing-Original Draft Preparation, F.C., R.R., S.C., and I.D.A. All authors have read and agreed to the final version of the manuscript.

Authors Information

German Benito:gbenitomenendez1@gmail.comhttps://orcid.org/0009-0000-2510-5237

Maria Luisa Massardi: marialuisa.massardi@unibs.it ORCID: 0009-0005-0718-9138

Serena Filiberti: s.filiberti@studenti.unibs.it ORCID: 0000-0001-9795-2638

Roberto Ronca: roberto.ronca@unibs.it ORCID: 0000-0001-8979-7068

Rahime Simsek: rsimsek@hacettepe.edu.tr ORCID: 0000-0002-8467-6336

Gioele Renzi: gioele.renzi@unifi.it https://orcid.org/0009-0008-9109-030X

Marialuigia Fantacuzzi: marialuigia.fantacuzzi@unich.it https://orcid.org/0000-0003-2401-7547

Ilaria D'Agostino: ilaria.dagostino@unipi.it ORCID: orcid.org/0000-0002-4870-7326

Simone Carradori: simone.carradori@unich.it http://orcid.org/0000-0002-8698-9440

Fabrizio Carta: fabrizio.carta@unifi.it http://orcid.org/0000-0002-1141-6146

Andrea Angeli: andrea.angeli@unifi.it https://orcid.org/0000-0002-1470-7192

Clemente Capasso: clemente.capasso@ibbr.cnr.it https://orcid.org/0000-0003-3314-2411

Claudiu T. Supuran: claudiu.supuran@unifi.it https://orcid.org/0000-0003-4262-0323

Conflicts of Interest

There are no conflicts of interest to declare.

Acknowledgments

REFERENCES

[1] Brown JS, Amend SR, Austin RH, Gatenby RA, Hammarlund EU, Pienta KJ. Updating the Definition of Cancer. Mol Cancer Res 2023;21:1142–7. https://doi.org/10.1158/1541-7786.MCR-23-0411.

[2] Magrassi L, Pinton G, Luzzi S, Comincini S, Scravaglieri A, Gigliotti V, et al. A New Vista of Aldehyde Dehydrogenase 1A3 (ALDH1A3): New Specific Inhibitors and Activity-Based Probes Targeting ALDH1A3 Dependent Pathways in Glioblastoma, Mesothelioma and Other Cancers. Cancers 2024;16:2397. https://doi.org/10.3390/cancers16132397.

[3] Global Cancer Observatory n.d. https://gco.iarc.fr/en (accessed January 6, 2025).

[4] Global cancer burden growing, amidst mounting need for services n.d. https://www.who.int/news/item/01-02-2024-global-cancer-burden-growing--amidst-mounting-need-for-services (accessed January 6, 2025).

[5] Anand U, Dey A, Chandel AKS, Sanyal R, Mishra A, Pandey DK, et al. Cancer chemotherapy and beyond: Current status, drug candidates, associated risks and progress in targeted therapeutics. Genes Dis 2023;10:1367–401. https://doi.org/10.1016/j.gendis.2022.02.007.

[6] Zafar A, Khan MJ, Abu J, Naeem A. Revolutionizing cancer care strategies: immunotherapy, gene therapy, and molecular targeted therapy. Mol Biol Rep 2024;51:219. https://doi.org/10.1007/s11033-023-09096-8.

[7] Zhong L, Li Y, Xiong L, Wang W, Wu M, Yuan T, et al. Small molecules in targeted cancer therapy: advances, challenges, and future perspectives. Signal Transduct Target Ther 2021;6:1–48. https://doi.org/10.1038/s41392-021-00572-w.

[8] Liu G, Chen T, Zhang X, Ma X, Shi H. Small molecule inhibitors targeting the cancers. MedComm 2022;3:e181. https://doi.org/10.1002/mco2.181.

[9] Li R, Ma X-L, Gou C, Tse WKF. Editorial: Novel small molecules in targeted cancer therapy. Front Pharmacol 2023;14. https://doi.org/10.3389/fphar.2023.1272523.

[10] Talevi A. Multi-target pharmacology: possibilities and limitations of the "skeleton key approach" from a medicinal chemist perspective. Front Pharmacol 2015;6:205. https://doi.org/10.3389/fphar.2015.00205.

[11] Makhoba XH, Viegas Jr C, Mosa RA, Viegas FPD, Pooe OJ. Potential Impact of the Multi-Target Drug Approach in the Treatment of Some Complex Diseases. Drug Des Devel Ther 2020;14:3235–49. https://doi.org/10.2147/DDDT.S257494.

[12] Doostmohammadi A, Jooya H, Ghorbanian K, Gohari S, Dadashpour M. Potentials and future perspectives of multi-target drugs in cancer treatment: the next generation anti-cancer agents. Cell Commun Signal CCS 2024;22:228. https://doi.org/10.1186/s12964-024-01607-9.

[13]   Zhao Q, Huang G. 7 - Anticancer Hybrids. In: Decker M, editor. Des. Hybrid Mol. Drug Dev., Elsevier; 2017, p. 193–218. https://doi.org/10.1016/B978-0-08-101011-2.00007-6.

[14]   Szumilak M, Wiktorowska-Owczarek A, Stanczak A. Hybrid Drugs-A Strategy for Overcoming Anticancer Drug Resistance? Mol Basel Switz 2021;26:2601. https://doi.org/10.3390/molecules26092601.

[15]   Shalini null, Kumar V. Have molecular hybrids delivered effective anti-cancer treatments and what should future drug discovery focus on? Expert Opin Drug Discov 2021;16:335–63. https://doi.org/10.1080/17460441.2021.1850686.

[16]   Alkhzem AH, Woodman TJ, Blagbrough IS. Design and synthesis of hybrid compounds as novel drugs and medicines. RSC Adv 2022;12:19470–84. https://doi.org/10.1039/d2ra03281c.

[17]   Shagufta, Ahmad I. Therapeutic significance of molecular hybrids for breast cancer research and treatment. RSC Med Chem 2023;14:218–38. https://doi.org/10.1039/D2MD00356B.

[18]   Ma XH, Shi Z, Tan C, Jiang Y, Go ML, Low BC, et al. In-silico approaches to multi-target drug discovery : computer aided multi-target drug design, multi-target virtual screening. Pharm Res 2010;27:739–49. https://doi.org/10.1007/s11095-010-0065-2.

[19]   Singh AK, Kumar A, Singh H, Sonawane P, Paliwal H, Thareja S, et al. Concept of Hybrid Drugs and Recent Advancements in Anticancer Hybrids. Pharm Basel Switz 2022;15:1071. https://doi.org/10.3390/ph15091071.

[20]   Sampath Kumar HM, Herrmann L, Tsogoeva SB. Structural hybridization as a facile approach to new drug candidates. Bioorg Med Chem Lett 2020;30:127514. https://doi.org/10.1016/j.bmcl.2020.127514.

[21]   Zhang G, Fang L, Zhu L, Sun D, Wang PG. Syntheses and biological activity of bisdaunorubicins. Bioorg Med Chem 2006;14:426–34. https://doi.org/10.1016/j.bmc.2005.08.014.

[22]   Kerru N, Singh P, Koorbanally N, Raj R, Kumar V. Recent advances (2015–2016) in anticancer hybrids. Eur J Med Chem 2017;142:179–212. https://doi.org/10.1016/j.ejmech.2017.07.033.

[23]   Moiseeva AA, Artyushin OI, Anikina LV, Brel VK. Synthesis and antitumor activity of daunorubicin conjugates with of 3,4-methylendioxybenzaldehyde. Bioorg Med Chem Lett 2019;29:126617. https://doi.org/10.1016/j.bmcl.2019.08.021.

[24]   Feng L-S, Su W-Q, Cheng J-B, Xiao T, Li H-Z, Chen D-A, et al. Benzimidazole hybrids as anticancer drugs: An updated review on anticancer properties, structure–activity relationship, and mechanisms of action (2019–2021). Arch Pharm (Weinheim) 2022;355:2200051. https://doi.org/10.1002/ardp.202200051.

[25]   Beckers T, Mahboobi S, Sellmer A, Winkler M, Eichhorn E, Pongratz H, et al. Chimerically designed HDAC- and tyrosine kinase inhibitors. A series of erlotinib hybrids as dual-selective inhibitors of EGFR, HER2 and histone deacetylases. MedChemComm 2012;3:829–35. https://doi.org/10.1039/C2MD00317A.

[26]   Zhang Y, Tortorella MD, Liao J, Qin X, Chen T, Luo J, et al. Synthesis and Evaluation of Novel Erlotinib–NSAID Conjugates as More Comprehensive Anticancer Agents. ACS Med Chem Lett 2015;6:1086–90. https://doi.org/10.1021/acsmedchemlett.5b00286.

[27]   Wei Y, Poon DC, Fei R, Lam ASM, Au-Yeung SCF, To KKW. A platinum-based hybrid drug design approach to circumvent acquired resistance to molecular targeted tyrosine kinase inhibitors. Sci Rep 2016;6:25363. https://doi.org/10.1038/srep25363.

[28]   Alam MdM, Hassan AHE, Lee KW, Cho MC, Yang JS, Song J, et al. Design, synthesis and cytotoxicity of chimeric erlotinib-alkylphospholipid hybrids. Bioorganic Chem 2019;84:51–62. https://doi.org/10.1016/j.bioorg.2018.11.021.

[29]   Ortega E, Zamora A, Basu U, Lippmann P, Rodríguez V, Janiak C, et al. An Erlotinib gold(I) conjugate for combating triple-negative breast cancer. J Inorg Biochem 2020;203:110910. https://doi.org/10.1016/j.jinorgbio.2019.110910.

[30]   Biegański P, Godel M, Riganti C, Kawano DF, Kopecka J, Kowalski K. Click ferrocenyl-erlotinib conjugates active against erlotinib-resistant non-small cell lung cancer cells *in vitro*. Bioorganic Chem 2022;119:105514. https://doi.org/10.1016/j.bioorg.2021.105514.

RSC Medicinal Chemistry Accepted Manuscript

[31] Murányi J, Duró C, Gurbi B, Móra I, Varga A, Németh K, et al. Novel Erlotinib–Chalcone Hybrids Diminish Resistance in Head and Neck Cancer by Inducing Multiple Cell Death Mechanisms. Int J Mol Sci 2023;24:3456. https://doi.org/10.3390/ijms24043456.

[32] Biegański P, Gazecka M, Nowak R, Gorski A, Dutkiewicz N, Kawano DF, et al. Organometallic–Erlotinib Conjugates Active against Lung Cancer Cells and as Emerging Virus Entry Inhibitors. Organometallics 2024;43:2505–19. https://doi.org/10.1021/acs.organomet.4c00145.

[33] Singh D, Attri BK, Gill RK, Bariwal J. Review on EGFR Inhibitors: Critical Updates. Mini Rev Med Chem 2016;16:1134–66. https://doi.org/10.2174/1389557516666160321114917.

[34] Steins M, Thomas M, Geißler M. Erlotinib. In: Martens UM, editor. Small Mol. Oncol., Cham: Springer International Publishing; 2018, p. 1–17. https://doi.org/10.1007/978-3-319-91442-8_1.

[35] Minna JD, Dowell J. Erlotinib hydrochloride. Nat Rev Drug Discov 2005;Suppl:S14-15. https://doi.org/10.1038/nrd1612.

[36] Gazdar AF. Personalized medicine and inhibition of EGFR signaling in lung cancer. N Engl J Med 2009;361:1018–20. https://doi.org/10.1056/NEJMe0905763.

[37] Baumgartner U, Berger F, Hashemi Gheinani A, Burgener SS, Monastyrskaya K, Vassella E. miR-19b enhances proliferation and apoptosis resistance via the EGFR signaling pathway by targeting PP2A and BIM in non-small cell lung cancer. Mol Cancer 2018;17:44. https://doi.org/10.1186/s12943-018-0781-5.

[38] Levantini E, Maroni G, Del Re M, Tenen DG. EGFR signaling pathway as therapeutic target in human cancers. Semin Cancer Biol 2022;85:253–75. https://doi.org/10.1016/j.semcancer.2022.04.002.

[39] Sainsbury JR, Farndon JR, Needham GK, Malcolm AJ, Harris AL. Epidermal-growth-factor receptor status as predictor of early recurrence of and death from breast cancer. Lancet Lond Engl 1987;1:1398–402. https://doi.org/10.1016/s0140-6736(87)90593-9.

[40] Salomon DS, Brandt R, Ciardiello F, Normanno N. Epidermal growth factor-related peptides and their receptors in human malignancies. Crit Rev Oncol Hematol 1995;19:183–232. https://doi.org/10.1016/1040-8428(94)00144-i.

[41] Burness ML, Grushko TA, Olopade OI. Epidermal growth factor receptor in triple-negative and basal-like breast cancer: promising clinical target or only a marker? Cancer J Sudbury Mass 2010;16:23–32. https://doi.org/10.1097/PPO.0b013e3181d24fc1.

[42] Stamos J, Sliwkowski MX, Eigenbrot C. Structure of the Epidermal Growth Factor Receptor Kinase Domain Alone and in Complex with a 4-Anilinoquinazoline Inhibitor *. J Biol Chem 2002;277:46265–72. https://doi.org/10.1074/jbc.M207135200.

[43] Park JH, Liu Y, Lemmon MA, Radhakrishnan R. Erlotinib binds both inactive and active conformations of the EGFR tyrosine kinase domain. Biochem J 2012;448:417–23. https://doi.org/10.1042/BJ20121513.

[44] Sun G, Mao L, Deng W, Xu S, Zhao J, Yang J, et al. Discovery of a Series of 1,2,3-Triazole-Containing Erlotinib Derivatives With Potent Anti-Tumor Activities Against Non-Small Cell Lung Cancer. Front Chem 2022;9. https://doi.org/10.3389/fchem.2021.789030.

[45] Mao L, Wang Z-Z, Wu Q, Chen X, Yang J-X, Wang X, et al. Design, Synthesis, and Antitumor Activity of Erlotinib Derivatives. Front Pharmacol 2022;13. https://doi.org/10.3389/fphar.2022.849364.

[46] Deng P, Sun G, Zhao J, Yao K, Yuan M, Peng L, et al. Synthesis and Antitumor Activity of Erlotinib Derivatives Linked With 1,2,3-Triazole. Front Pharmacol 2022;12:793905. https://doi.org/10.3389/fphar.2021.793905.

[47] Gao Y, Zhang H, Zhang Y, Lv T, Zhang L, Li Z, et al. Erlotinib-Guided Self-Assembled Trifunctional Click Nanotheranostics for Distinguishing Druggable Mutations and Synergistic Therapy of Nonsmall Cell Lung Cancer. Mol Pharm 2018;15:5146–61. https://doi.org/10.1021/acs.molpharmaceut.8b00561.

[48] Bonandi E, Christodoulou MS, Fumagalli G, Perdicchia D, Rastelli G, Passarella D. The 1,2,3-triazole ring as a bioisostere in medicinal chemistry. Drug Discov Today 2017;22:1572–81. https://doi.org/10.1016/j.drudis.2017.05.014.

[49]   Khandelwal R, Vasava M, Abhirami RB, Karsharma M. Recent advances in triazole synthesis via click chemistry and their pharmacological applications: A review. Bioorg Med Chem Lett 2024;112:129927. https://doi.org/10.1016/j.bmcl.2024.129927.

[50]   Supuran CT. A simple yet multifaceted 90 years old, evergreen enzyme: Carbonic anhydrase, its inhibition and activation. Bioorg Med Chem Lett 2023;93:129411. https://doi.org/10.1016/j.bmcl.2023.129411.

[51]   Baroni C, D'Agostino I, Renzi G, Kilbile JT, Tamboli Y, Ferraroni M, et al. Lasamide, a Potent Human Carbonic Anhydrase Inhibitor from the Market: Inhibition Profiling and Crystallographic Studies. ACS Med Chem Lett 2024;15:1749–55. https://doi.org/10.1021/acsmedchemlett.4c00341.

[52]   D'Agostino I, Bonardi A, Ferraroni M, Gratteri P, Angeli A, Supuran CT. Exploring the Polypharmacological Potential of PCI-27483: A Selective Inhibitor of Carbonic Anhydrases IX and XII. ACS Med Chem Lett 2024;15:2042–5. https://doi.org/10.1021/acsmedchemlett.4c00443.

[53]   Mishra CB, Tiwari M, Supuran CT. Progress in the development of human carbonic anhydrase inhibitors and their pharmacological applications: Where are we today? Med Res Rev 2020;40:2485–565. https://doi.org/10.1002/med.21713.

[54]   D'Ambrosio K, Di Fiore A, Alterio V, Langella E, Monti SM, Supuran CT, et al. Multiple Binding Modes of Inhibitors to Human Carbonic Anhydrases: An Update on the Design of Isoform-Specific Modulators of Activity. Chem Rev 2024. https://doi.org/10.1021/acs.chemrev.4c00278.

[55]   Denner TC, Angeli A, Ferraroni M, Supuran CT, Csuk R. Ureidobenzenesulfonamides as Selective Carbonic Anhydrase I, IX, and XII Inhibitors. Mol Basel Switz 2023;28:7782. https://doi.org/10.3390/molecules28237782.

[56]   Supuran CT. Carbonic anhydrase inhibitors and their potential in a range of therapeutic areas. Expert Opin Ther Pat 2018;28:709–12. https://doi.org/10.1080/13543776.2018.1523897.

[57]   De Simone G, Supuran CT. Anticancer drugs: where are we now? Expert Opin Ther Pat 2024;34:525–7. https://doi.org/10.1080/13543776.2024.2353625.

[58]   Kilbile JT, Sapkal SB, Renzi G, D'Agostino I, Boudjelal M, Tamboli Y, et al. Lasamide Containing Sulfonylpiperazines as Effective Agents for the Management of Glaucoma Associated Symptoms. ChemMedChem 2024;19:e202400601. https://doi.org/10.1002/cmdc.202400601.

[59]   Ronca R, Supuran CT. Carbonic anhydrase IX: An atypical target for innovative therapies in cancer. Biochim Biophys Acta Rev Cancer 2024;1879:189120. https://doi.org/10.1016/j.bbcan.2024.189120.

[60]   Aslan H, Renzi G, Angeli A, D'Agostino I, Ronca R, Massardi M, et al. Benzenesulfonamide Decorated Dihydropyrimidin(thi)ones: Carbonic Anhydrase Profiling and Antiproliferative Activity. RSC Med Chem 2024;15:1929–41. https://doi.org/10.1039/D4MD00101J.

[61]   Abdoli M, Bonardi A, Supuran CT, Žalubovskis R. Synthesis and Carbonic Anhydrase I, II, IX, and XII Inhibition Studies with a Series of Cyclic Sulfonyl Guanidines. ChemMedChem 2024;19:e202400197. https://doi.org/10.1002/cmdc.202400197.

[62]   Angeli A, Chelli I, Lucarini L, Sgambellone S, Marri S, Villano S, et al. Novel Carbonic Anhydrase Inhibitors with Dual-Tail Core Sulfonamide Show Potent and Lasting Effects for Glaucoma Therapy. J Med Chem 2024;67:3066–89. https://doi.org/10.1021/acs.jmedchem.3c02254.

[63]   Angeli A, Petrou A, Kartsev VG, Zubenko A, Divaeva LN, Chekrisheva V, et al. Phthalazine Sulfonamide Derivatives as Carbonic Anhydrase Inhibitors. Synthesis, Biological and *in silico* Evaluation. ChemMedChem 2024:e202400147. https://doi.org/10.1002/cmdc.202400147.

[64]   Benito G, D'Agostino I, Carradori S, Fantacuzzi M, Agamennone M, Puca V, et al. Erlotinib-containing benzenesulfonamides as anti-Helicobacter pylori agents through carbonic anhydrase inhibition. Future Med Chem 2023;15:1865–83. https://doi.org/10.4155/fmc-2023-0208.

[65] Gumus A, D'Agostino I, Puca V, Crocetta V, Carradori S, Cutarella L, et al. Cyclization of acyl thiosemicarbazides led to new Helicobacter pylori α-carbonic anhydrase inhibitors. Arch Pharm (Weinheim) 2024;357:e2400548. https://doi.org/10.1002/ardp.202400548.

[66] Doléans-Jordheim A, Bergeron E, Bereyziat F, Ben-Larbi S, Dumitrescu O, Mazoyer M-A, et al. Zidovudine (AZT) has a bactericidal effect on enterobacteria and induces genetic modifications in resistant strains. Eur J Clin Microbiol Infect Dis Off Publ Eur Soc Clin Microbiol 2011;30:1249–56. https://doi.org/10.1007/s10096-011-1220-3.

[67] Elwell LP, Ferone R, Freeman GA, Fyfe JA, Hill JA, Ray PH, et al. Antibacterial activity and mechanism of action of 3'-azido-3'-deoxythymidine (BW A509U). Antimicrob Agents Chemother 1987;31:274–80. https://doi.org/10.1128/AAC.31.2.274.

[68] Bernardoni BL, La Motta C, Carradori S, D'Agostino I. Helicobacter pylori CAs inhibition. The Enzymes 2024;55:213–41. https://doi.org/10.1016/bs.enz.2024.05.013.

[69] Supuran CT. Novel carbonic anhydrase inhibitors for the treatment of Helicobacter pylori infection. Expert Opin Investig Drugs 2024:1–10. https://doi.org/10.1080/13543784.2024.2334714.

[70] Kim J, Kim N, Park JH, Chang H, Kim JY, Lee DH, et al. The Effect of Helicobacter pylori on Epidermal Growth Factor Receptor-Induced Signal Transduction and the Preventive Effect of Celecoxib in Gastric Cancer Cells. Gut Liver 2013;7:552–9. https://doi.org/10.5009/gnl.2013.7.5.552.

[71] Chichirau BE, Diechler S, Posselt G, Wessler S. Tyrosine Kinases in Helicobacter pylori Infections and Gastric Cancer. Toxins 2019;11:591. https://doi.org/10.3390/toxins11100591.

[72] Khalifah RG. The carbon dioxide hydration activity of carbonic anhydrase. I. Stop-flow kinetic studies on the native human isoenzymes B and C. J Biol Chem 1971;246:2561–73.

[73] Liguori F, Carradori S, Ronca R, Rezzola S, Filiberti S, Carta F, et al. Benzenesulfonamides with different rigidity-conferring linkers as carbonic anhydrase inhibitors: an insight into the antiproliferative effect on glioblastoma, pancreatic, and breast cancer cells. J Enzyme Inhib Med Chem 2022;37:1857–69. https://doi.org/10.1080/14756366.2022.2091557.

[74] Ciccone V, Filippelli A, Angeli A, Supuran CT, Morbidelli L. Pharmacological Inhibition of CA-IX Impairs Tumor Cell Proliferation, Migration and Invasiveness. Int J Mol Sci 2020;21:2983. https://doi.org/10.3390/ijms21082983.

[75] Ali S, El-Rayes BF, Sarkar FH, Philip PA. Simultaneous targeting of the epidermal growth factor receptor and cyclooxygenase-2 pathways for pancreatic cancer therapy. Mol Cancer Ther 2005;4:1943–51. https://doi.org/10.1158/1535-7163.MCT-05-0065.

[76] Deng C, Xiong J, Gu X, Chen X, Wu S, Wang Z, et al. Novel recombinant immunotoxin of EGFR specific nanobody fused with cucurmosin, construction and antitumor efficiency in vitro. Oncotarget 2017;8:38568–80. https://doi.org/10.18632/oncotarget.16930.

[77] Vagaggini C, Petroni D, D'Agostino I, Poggialini F, Cavallini C, Cianciusi A, et al. Early investigation of a novel SI306 theranostic prodrug for glioblastoma treatment. Drug Dev Res 2024;85:e22158. https://doi.org/10.1002/ddr.22158.

[78] Li W, Zhan P, De Clercq E, Lou H, Liu X. Current drug research on PEGylation with small molecular agents. Prog Polym Sci 2013;38:421–44. https://doi.org/10.1016/j.progpolymsci.2012.07.006.

[79] Veronese FM, Mero A. The impact of PEGylation on biological therapies. BioDrugs Clin Immunother Biopharm Gene Ther 2008;22:315–29. https://doi.org/10.2165/00063030-200822050-00004.

[80] Greenwald RB. PEG drugs: an overview. J Control Release Off J Control Release Soc 2001;74:159–71. https://doi.org/10.1016/s0168-3659(01)00331-5.

[81] Chey WD, Webster L, Sostek M, Lappalainen J, Barker PN, Tack J. Naloxegol for Opioid-Induced Constipation in Patients with Noncancer Pain. N Engl J Med 2014;370:2387–96. https://doi.org/10.1056/NEJMoa1310246.

[82] Liu J, Zahedi P, Zeng F, Allen C. Nano-sized assemblies of a PEG-docetaxel conjugate as a formulation strategy for docetaxel. J Pharm Sci 2008;97:3274–90. https://doi.org/10.1002/jps.21245.

[83] Omar R, Bardoogo YL, Corem-Salkmon E, Mizrahi B. Amphiphilic star PEG-Camptothecin conjugates for intracellular targeting. J Control Release Off J Control Release Soc 2017;257:76–83. https://doi.org/10.1016/j.jconrel.2016.09.025.

RSC Medicinal Chemistry Accepted Manuscript

[84] Park EJ, Choi J, Lee KC, Na DH. Emerging PEGylated non-biologic drugs. Expert Opin Emerg Drugs 2019;24:107–19. https://doi.org/10.1080/14728214.2019.1604684.

[85] Bebbington D, Dawson CE, Gaur S, Spencer J. Prodrug and covalent linker strategies for the solubilization of dual-Action antioxidants/Iron chelators. Bioorg Med Chem Lett 2002;12:3297–300. https://doi.org/10.1016/S0960-894X(02)00698-4.

[86] Troup RI, Fallan C, Baud MGJ. Current strategies for the design of PROTAC linkers: a critical review. Explor Target Anti-Tumor Ther 2020;1:273–312. https://doi.org/10.37349/etat.2020.00018.

[87] Li Q, Li W, Xu K, Xing Y, Shi H, Jing Z, et al. PEG Linker Improves Antitumor Efficacy and Safety of Affibody-Based Drug Conjugates. Int J Mol Sci 2021;22:1540. https://doi.org/10.3390/ijms22041540.

[88] Ma Y, Fang Z, Zhang H, Qi Y, Mao Y, Zheng J. PDZK1 suppresses TNBC development and sensitizes TNBC cells to erlotinib via the EGFR pathway. Cell Death Dis 2024;15:1–14. https://doi.org/10.1038/s41419-024-06502-2.

[89] Foulkes WD, Smith IE, Reis-Filho JS. Triple-negative breast cancer. N Engl J Med 2010;363:1938–48. https://doi.org/10.1056/NEJMra1001389.

[90] Gluz O, Liedtke C, Gottschalk N, Pusztai L, Nitz U, Harbeck N. Triple-negative breast cancer--current status and future directions. Ann Oncol Off J Eur Soc Med Oncol 2009;20:1913–27. https://doi.org/10.1093/annonc/mdp492.

[91] Rodríguez-Pinilla SM, Sarrió D, Honrado E, Moreno-Bueno G, Hardisson D, Calero F, et al. Vimentin and laminin expression is associated with basal-like phenotype in both sporadic and BRCA1-associated breast carcinomas. J Clin Pathol 2007;60:1006–12. https://doi.org/10.1136/jcp.2006.042143.

[92] Sarrió D, Rodriguez-Pinilla SM, Hardisson D, Cano A, Moreno-Bueno G, Palacios J. Epithelial-mesenchymal transition in breast cancer relates to the basal-like phenotype. Cancer Res 2008;68:989–97. https://doi.org/10.1158/0008-5472.CAN-07-2017.

[93] Liu Z, He K, Ma Q, Yu Q, Liu C, Ndege I, et al. Autophagy inhibitor facilitates gefitinib sensitivity in vitro and in vivo by activating mitochondrial apoptosis in triple negative breast cancer. PloS One 2017;12:e0177694. https://doi.org/10.1371/journal.pone.0177694.

[94] Yamasaki F, Zhang D, Bartholomeusz C, Sudo T, Hortobagyi GN, Kurisu K, et al. Sensitivity of breast cancer cells to erlotinib depends on cyclin-dependent kinase 2 activity. Mol Cancer Ther 2007;6:2168–77. https://doi.org/10.1158/1535-7163.MCT-06-0514.

[95] Fenn K, Maurer M, Lee SM, Crew KD, Trivedi MS, Accordino MK, et al. Phase 1 Study of Erlotinib and Metformin in Metastatic Triple-Negative Breast Cancer. Clin Breast Cancer 2020;20:80–6. https://doi.org/10.1016/j.clbc.2019.08.004.

[96] Ueno NT, Zhang D. Targeting EGFR in Triple Negative Breast Cancer. J Cancer 2011;2:324–8. https://doi.org/10.7150/jca.2.324.

[97] Lefebvre C, Pellizzari S, Bhat V, Jurcic K, Litchfield DW, Allan AL. Involvement of the AKT Pathway in Resistance to Erlotinib and Cabozantinib in Triple-Negative Breast Cancer Cell Lines. Biomedicines 2023;11:2406. https://doi.org/10.3390/biomedicines11092406.

[98] Dickler MN, Rugo HS, Eberle CA, Brogi E, Caravelli JF, Panageas KS, et al. A Phase II Trial of Erlotinib in Combination with Bevacizumab in Patients with Metastatic Breast Cancer. Clin Cancer Res Off J Am Assoc Cancer Res 2008;14:7878–83. https://doi.org/10.1158/1078-0432.CCR-08-0141.

[99] Ricciardi S, Tomao S, de Marinis F. Efficacy and safety of erlotinib in the treatment of metastatic non-small-cell lung cancer. Lung Cancer Targets Ther 2010;2:1–9. https://doi.org/10.2147/LCTT.S10167.

[100] Tolaney SM, Nechushtan H, Ron I-G, Schöffski P, Awada A, Yasenchak CA, et al. Cabozantinib for metastatic breast carcinoma: results of a phase II placebo-controlled randomized discontinuation study. Breast Cancer Res Treat 2016;160:305–12. https://doi.org/10.1007/s10549-016-4001-y.

[101] Bao B, Mitrea C, Wijesinghe P, Marchetti L, Girsch E, Farr RL, et al. Treating triple negative breast cancer cells with erlotinib plus a select antioxidant overcomes drug resistance by targeting cancer cell heterogeneity. Sci Rep 2017;7:44125. https://doi.org/10.1038/srep44125.

RSC Medicinal Chemistry Accepted Manuscript

[102] Schiavon E, Rezzola S, Filippi E, Turati M, Parrasia S, Bernardotto S, et al. A novel mertansine conjugate for acid-reversible targeted drug delivery validated through the Avidin-Nucleic-Acid-NanoASsembly platform. Nanomedicine Nanotechnol Biol Med 2024;62:102784. https://doi.org/10.1016/j.nano.2024.102784.

[103] Ali M, Bozdag M, Farooq U, Angeli A, Carta F, Berto P, et al. Benzylaminoethyureido-Tailed Benzenesulfonamides: Design, Synthesis, Kinetic and X-ray Investigations on Human Carbonic Anhydrases. Int J Mol Sci 2020;21:2560. https://doi.org/10.3390/ijms21072560.

[104] Ali M, Angeli A, Bozdag M, Carta F, Capasso C, Farooq U, et al. Benzylaminoethylureido-Tailed Benzenesulfonamides Show Potent Inhibitory Activity against Bacterial Carbonic Anhydrases. ChemMedChem 2020;15:2444–7. https://doi.org/10.1002/cmdc.202000680.

[105] Bonardi A, Nocentini A, Giovannuzzi S, Paoletti N, Ammara A, Bua S, et al. Development of Penicillin-Based Carbonic Anhydrase Inhibitors Targeting Multidrug-Resistant Neisseria gonorrhoeae. J Med Chem 2024;67:9613–27. https://doi.org/10.1021/acs.jmedchem.4c00740.

[106] Bozdag M, Alafeefy AM, Carta F, Ceruso M, Al-Tamimi A-MS, Al-Kahtani AA, et al. Synthesis 4-[2-(2-mercapto-4-oxo-4H-quinazolin-3-yl)-ethyl]-benzenesulfonamides with subnanomolar carbonic anhydrase II and XII inhibitory properties. Bioorg Med Chem 2016;24:4100–7. https://doi.org/10.1016/j.bmc.2016.06.052.

[107] Kumar A, Siwach K, Supuran CT, Sharma PK. A decade of tail-approach based design of selective as well as potent tumor associated carbonic anhydrase inhibitors. Bioorganic Chem 2022;126:105920. https://doi.org/10.1016/j.bioorg.2022.105920.

[108] Bonardi A, Nocentini A, Giovannuzzi S, Paoletti N, Ammara A, Bua S, et al. Development of Penicillin-Based Carbonic Anhydrase Inhibitors Targeting Multidrug-Resistant Neisseria gonorrhoeae. J Med Chem 2024;67:9613–27. https://doi.org/10.1021/acs.jmedchem.4c00740.

[109] Carta F, Akdemir A, Scozzafava A, Masini E, Supuran CT. Xanthates and Trithiocarbonates Strongly Inhibit Carbonic Anhydrases and Show Antiglaucoma Effects in Vivo. J Med Chem 2013;56:4691–700. https://doi.org/10.1021/jm400414j.

[110] Marinacci B, D'Agostino I, Angeli A, Carradori S, Melfi F, Grande R, et al. Inhibition of Pseudomonas aeruginosa Carbonic Anhydrases, Exploring Ciprofloxacin Functionalization Toward New Antibacterial Agents: An In-Depth Multidisciplinary Study. J Med Chem 2024. https://doi.org/10.1021/acs.jmedchem.4c01555.

[111] Baell JB, Nissink JWM. Seven Year Itch: Pan-Assay Interference Compounds (PAINS) in 2017—Utility and Limitations. ACS Chem Biol 2018;13:36–44. https://doi.org/10.1021/acschembio.7b00903.

[112] Daina A, Michielin O, Zoete V. SwissADME: a free web tool to evaluate pharmacokinetics, drug-likeness and medicinal chemistry friendliness of small molecules. Sci Rep 2017;7:42717. https://doi.org/10.1038/srep42717.

[113] Balestri LJI, D'Agostino I, Rango E, Vagaggini C, Marchitiello R, Mariotti M, et al. Focused library of phenyl-fused macrocyclic amidinoureas as antifungal agents. Mol Divers 2022;26:3399–409. https://doi.org/10.1007/s11030-022-10388-7.

[114] D'Agostino I, Mathew GE, Angelini P, Venanzoni R, Angeles Flores G, Angeli A, et al. Biological investigation of N-methyl thiosemicarbazones as antimicrobial agents and bacterial carbonic anhydrases inhibitors. J Enzyme Inhib Med Chem 2022;37:986–93. https://doi.org/10.1080/14756366.2022.2055009.

[115] Redij A, Carradori S, Petreni A, Supuran CT, Toraskar MP. Coumarin-pyrazoline Hybrids as Selective Inhibitors of the Tumor-associated Carbonic Anhydrase IX and XII. Anticancer Agents Med Chem 2023;23:1217–23. https://doi.org/10.2174/1871520623666230220162506.

[116] Schrödinger Release 2024-1. Maestro, Glide, Protein Preparation Wizard, Epik, MacroModel, Prime. New York (NY): Schrödinger, LLC; 2024 n.d.

[117] Greenwood JR, Calkins D, Sullivan AP, Shelley JC. Towards the comprehensive, rapid, and accurate prediction of the favorable tautomeric states of drug-like molecules in aqueous solution. J Comput Aided Mol Des 2010;24:591–604. https://doi.org/10.1007/s10822-010-9349-1.

[118] Bozdag M, Ferraroni M, Ward C, Carta F, Bua S, Angeli A, et al. Carbonic anhydrase inhibitors based on sorafenib scaffold: Design, synthesis, crystallographic investigation and effects on primary breast cancer cells. Eur J Med Chem 2019;182:111600. https://doi.org/10.1016/j.ejmech.2019.111600.

[119] Leitans J, Kazaks A, Bogans J, Supuran CT, Akopjana I, Ivanova J, et al. Structural Basis of Saccharin Derivative Inhibition of Carbonic Anhydrase IX. ChemMedChem 2023;18:e202300454. https://doi.org/10.1002/cmdc.202300454.

[120] Behnke CA, Le Trong I, Godden JW, Merritt EA, Teller DC, Bajorath J, et al. Atomic resolution studies of carbonic anhydrase II. Acta Crystallogr D Biol Crystallogr 2010;66:616–27. https://doi.org/10.1107/S0907444910006554.

[121] Čapkauskaitė E, Linkuvienė V, Smirnov A, Milinavičiūtė G, Timm DD, Kasiliauskaitė A, et al. Combinatorial Design of Isoform-Selective N-Alkylated Benzimidazole-Based Inhibitors of Carbonic Anhydrases. ChemistrySelect 2017;2:5360–71. https://doi.org/10.1002/slct.201700531.

[122] Sogabe S, Kawakita Y, Igaki S, Iwata H, Miki H, Cary DR, et al. Structure-Based Approach for the Discovery of Pyrrolo[3,2-d]pyrimidine-Based EGFR T790M/L858R Mutant Inhibitors. ACS Med Chem Lett 2013;4:201–5. https://doi.org/10.1021/ml300327z.

[123] Friesner RA, Banks JL, Murphy RB, Halgren TA, Klicic JJ, Mainz DT, et al. Glide: A New Approach for Rapid, Accurate Docking and Scoring. 1. Method and Assessment of Docking Accuracy. J Med Chem 2004;47:1739–49. https://doi.org/10.1021/jm0306430.

RSC Medicinal Chemistry Accepted Manuscript

The data supporting this article have been included as part of the Supplementary Information. The following data are made available in the ESI:

Selectivity index (SI) values for the first ERL-clicked derivatives (Table S1); Synthesis of compound 6 (Scheme S1); Procedure for the synthesis of compound 6); Antiproliferative effect of the first series of ERL clicked derivatives (Figure S1); 1H and 13C NMR of representative compounds.

The ESI file contains the NMR spectra of the compounds reported in this article.